

Manuscript prepared for Biogeosciences Discuss.  
with version 2.2 of the L<sup>A</sup>T<sub>E</sub>X class copernicus\_discussions.cls.  
Date: 1 July 2011

# **Sensitivity of atmospheric CO<sub>2</sub> and climate to explosive volcanic eruptions**

**T. L. Frölicher<sup>1,2,\*</sup>, F. Joos<sup>1,2</sup>, and C. C. Raible<sup>1,2</sup>**

<sup>1</sup>Climate and Environmental Physics, Physics Institute, University of Bern, Bern, Switzerland

<sup>2</sup>Oeschger Centre for Climate Change Research, University of Bern, Bern, Switzerland

\*now at: Program in Atmospheric and Oceanic Sciences, Princeton University, Princeton, USA

Correspondence to: T. L. Frölicher  
([tfrolich@princeton.edu](mailto:tfrolich@princeton.edu))

## Abstract

Impacts of low-latitude, explosive volcanic eruptions on climate and the carbon cycle are quantified by forcing a comprehensive, fully coupled carbon cycle-climate model with pulse-like stratospheric aerosol optical depth changes. The model represents the radiative and dynamical response of the climate system to volcanic eruptions and simulates a decrease of global and regional atmospheric surface temperature, regionally distinct changes in precipitation, a positive phase of the North Atlantic Oscillation, and a decrease in atmospheric CO<sub>2</sub> after volcanic eruptions. The volcanic-induced cooling reduces overturning rates in tropical soils, which dominates over reduced litter input due to soil moisture decrease, resulting in higher land carbon inventories for several decades. The perturbation in the ocean carbon inventory changes sign from an initial weak carbon sink to a carbon source. Positive carbon and negative temperature anomalies in subsurface waters last up to several decades. The multi-decadal decrease in atmospheric CO<sub>2</sub> yields a small additional radiative forcing that amplifies the cooling and perturbs the Earth System on longer time scales than the atmospheric residence time of volcanic aerosols. In addition, century-scale global warming simulations with and without volcanic eruptions over the historical period show that the ocean integrates volcanic radiative cooling and responds for different physical and biogeochemical parameters such as steric sea level or dissolved oxygen. Results from a suite of sensitivity simulations with different magnitudes of stratospheric aerosol optical depth changes and from global warming simulations show that the carbon cycle-climate sensitivity  $\gamma$ , expressed as change in atmospheric CO<sub>2</sub> per unit change in global mean surface temperature, depends on the magnitude and temporal evolution of the perturbation, and time scale of interest. On decadal time scales, modeled  $\gamma$  is several times larger for a Pinatubo-like eruption than for the industrial period and for a high emission, 21st century scenario.

## 1 Introduction

Variability on a wide range of time scales is present in the atmospheric CO<sub>2</sub> record from ice core and direct atmospheric samples. The main feature of the record, the long-term, centennial

rise in CO<sub>2</sub> is well understood and explained by anthropogenic emissions from fossil fuel and land use. However, the origin and underlying mechanisms of the substantial interannual-to-decadal scale variability in atmospheric CO<sub>2</sub> are less well quantified. External forcing such as volcanic eruptions as well as internal modes of variability such as the El-Niño/Southern Oscillation (Bacastow et al., 1980; Siegenthaler, 1990) contribute to the observed variability.

Variability has the potential to mask and to complicate the detection of the impacts of processes and feedbacks which are important for 21st century climate projections. Perhaps not surprisingly, different studies that investigate recent trends in the airborne fraction of anthropogenic emissions arrive at disparate conclusions on the feedback question even though analyzing the same data (Gloor et al., 2010; Sarmiento et al., 2010; Knorr, 2009; Quéré et al., 2009; Canadell et al., 2007, and other studies). It remains unclear whether the reconstructed changes in the fractions of anthropogenic carbon emissions absorbed by the ocean and land and in the fraction remaining in the atmosphere herald a decrease in the relative sink strength of the ocean and the land biosphere in response to long-term climate change and nonlinearities in the carbonate chemistry of ocean waters. Variability and related uncertainties also play a role when determining the magnitude and direction of climate-carbon cycle feedbacks (e.g., Plattner et al., 2008) as such uncertainties are suggested to be a major source for 21st century projections (Meehl et al., 2007). A recent probabilistic quantification of the sensitivity of atmospheric CO<sub>2</sub> to climate change from last millennium proxy data yields a broad distribution (Frank et al., 2010). This reflects various sources of uncertainties in the CO<sub>2</sub>-climate sensitivity including those arising from short-term variability and potentially differing carbon-climate sensitivities on different time scales and for different perturbations such as smoothly varying solar and greenhouse gas changes versus pulse-like volcanic aerosol spikes.

A better understanding of interannual-to-decadal scale variability is required if these important questions are to be resolved and if interannual-to-decadal scale processes are to be better distinguished from century-scale, anthropogenic trends. An important part of natural climate-carbon variability is caused by volcanic eruptions (cf. Fig. 1a in Sarmiento et al. (2010)) both during recent decades as well as during the preindustrial period. While the direct radiative and dynamical effects of sulfate aerosols from volcanic eruptions on the physical climate system

are relatively well known (e.g., [Robock, 2000](#); [Yoshimori et al., 2005](#); [Ammann et al., 2007](#)), less emphasis has been placed on investigating the impact of volcanic eruptions on the global carbon cycle and on variability in the CO<sub>2</sub> record (e.g., [Brovkin et al., 2010](#); [Jones and Cox, 2001](#); [Gerber et al., 2003](#)).

5 The purpose of this study is to assess the impact of volcanic eruptions on the coupled climate-biogeochemical system. The time scales of responses and changes in the atmosphere, terrestrial and ocean carbon inventories as well as the carbon cycle-climate sensitivity are quantified. The comprehensive fully coupled carbon cycle-climate system model NCAR CSM1.4-carbon is employed to capture the most important climate processes including non-linear feedbacks as well as radiative and dynamical processes. A suite of sensitivity simulations of low-latitude volcanic eruptions with different magnitudes of stratospheric aerosol optical depth changes are performed. Short- and long-term spatio-temporal changes in temperature, precipitation, and the marine and terrestrial carbon storage are investigated. Underlying mechanisms of marine and terrestrial carbon changes are presented. Our set of sensitivity and control simulations allows us to estimate the impact of volcanic eruptions on the land and ocean carbon cycle in comparison with unforced, internal Earth System variability in a self-consistent, 3-dimensional, dynamical setting and for different magnitudes of stratospheric aerosol optical depth changes. Furthermore, volcanic eruptions provide a suitable test bed to investigate the ability of Earth System models to respond realistically to global-scale radiative forcing perturbations.

10  
15  
20  
25 Large volcanic eruptions have long been known to substantially impact the climate system ([Franklin, 1784](#)). Explosive volcanic eruptions, such as the Mt Pinatubo eruption in June in year 1991, inject large amounts of SO<sub>2</sub> into the stratosphere and form sulfate aerosol clouds that persist for several years. Stratospheric sulphate aerosols clouds strongly interact with solar radiation. Light is scattered by aerosols and part of the incoming solar radiation is reflected back to space, thereby increasing the net planetary albedo, reducing the amount of solar energy that reaches the Earth's surface ([Humphreys, 1913](#)), and cooling the surface-troposphere system. A global surface cooling of about -0.49°C was observed after the Mt Pinatubo eruption in late 1992 ([Thompson et al., 2009](#)). In addition, dynamical effects led to an anomalous warm winter over the Northern Hemisphere continents due to a strengthening of the equator-to-pole

temperature gradient and accelerating polar vortex, which forced a positive phase of the North Atlantic Oscillation (NAO; e.g., [Shindell et al. \(2004\)](#)). Other effects of volcanic eruptions such as stratospheric ozone depletion and increase in diffuse radiation reaching the Earth surface are summarized in a review by [Robock \(2000\)](#).

5 Besides these physical effects, explosive volcanic eruptions substantially perturb the global carbon cycle. For example, the Mt Pinatubo eruption in 1991 was followed by a slowdown in the increase of atmospheric CO<sub>2</sub> for several years, entailing a weakening of the global warming trend ([Sarmiento et al., 2010](#)). The magnitude of the effect is even more remarkable when one considers that the 1991-1992 El-Niño should have led to a short-term increase in the growth rate  
10 of atmospheric CO<sub>2</sub>. The lower airborne fraction observed after the Pinatubo induced cooling is mainly attributed to terrestrial biosphere changes, and partly to oceanic changes ([Baker et al., 2006](#); [Rödenbeck et al., 2003](#); [Bousquet et al., 2000](#)). However, the exact role of biogeochemical mechanisms and of the time scales involved is difficult to constrain from inversion approaches and from observations due to their relatively sparse spatio-temporal coverage.

15 Model studies addressing the link between volcanic eruptions and the carbon cycle have so far used either atmosphere/land-only models forced with reanalysis data (e.g., [Angert et al., 2004](#); [Lucht et al., 2002](#)), or models with simplified setups ([Gerber et al., 2003](#)). [Angert et al. \(2004\)](#) used a biogeochemical model linked to an atmospheric tracer model to reject the idea that changes in diffuse radiation were responsible for the slowdown in the rise of atmospheric  
20 CO<sub>2</sub> after the Mt Pinatubo eruption. [Lucht et al. \(2002\)](#) attributed the atmospheric CO<sub>2</sub> changes after the Mt Pinatubo eruption to the effects of temperature on plant and soil respiration by using a dynamical vegetation model forced with observed climate data. Gerber and co-workers found a larger decrease in atmospheric CO<sub>2</sub> in simulations over the last millennium with than without volcanic forcing. These representations may miss some aspects of the fully coupled dynamical  
25 response to volcanic eruptions in the carbon cycle-climate system.

Fully coupled atmosphere-ocean general circulation models have been used to investigate ocean temperature, sea-level rise and heat content response to volcanic eruptions ([Delworth et al., 2005](#); [Gleckler et al., 2006](#); [Domingues et al., 2008](#); [Stenchikov et al., 2009](#)). Only a few studies employed fully coupled carbon cycle-climate model simulations to study the responses

of the carbon cycle to volcanic eruptions (Jones and Cox, 2001; Frölicher et al., 2009; Brovkin et al., 2010). Jones and Cox (2001) find that the surface cooling after the Mt Pinatubo eruption caused reduced soil and plant respiration globally for several years. Frölicher et al. (2009) describe the impact of volcanic eruptions on the dissolved oxygen concentration in the ocean. They find a significant long-term impact of volcanic eruptions on the subsurface dissolved oxygen concentration. Recently, Brovkin et al. (2010) have analyzed the largest eruption of the last millennium in 1258 AD in multiple-forcing ensemble simulations. They find a decline in atmospheric CO<sub>2</sub> due to reduced heterotrophic respiration on tropical and subtropical land regions similar to Jones and Cox (2001). Furthermore, they showed that the ocean acts as a weak carbon sink, which saturates a couple of years after the eruption. Characteristics of these two studies are that the carbon cycle anomalies simulated in the aftermath of the eruptions are also influenced by other time-varying forcings (Brovkin et al., 2010) or that the land model contains one soil pool only (Jones and Cox, 2001). In the study presented here, volcanic forcing is, to our knowledge for the first time, applied in isolation in a comprehensive coupled Earth System model to clearly distinguish its impact on the carbon cycle.

Important questions remain. How does the response of the climate-biogeochemical system scale with the strength of the explosive volcanic eruption? What are the regional fingerprints on the marine and terrestrial carbon cycle that arise solely as a result of volcanic radiative forcing? What are the mechanisms responsible for carbon inventory changes and what are the typical relaxation time scales of the carbon cycle to the relatively short-lived radiative forcing perturbation? Is the CO<sub>2</sub>-climate sensitivity the same for volcanic perturbations as for the anthropogenic climate perturbation? This study investigates these questions by using simulations with a comprehensive fully coupled carbon cycle-climate system model as such questions can typically not or not as easily be answered by (i) using cost-efficient EMIC's that do not represent internal variability and dynamical responses, by (ii) using AOGCM's without carbon cycle processes, or by (iii) analyzing existing millennium or IPCC-class simulations.

The outline is as follows. In the next section, the NCAR CSM1.4-carbon model and the experimental design are presented. In section 3a, global mean changes in volcanic forcings, surface temperature, atmospheric CO<sub>2</sub>, and in terrestrial and marine carbon inventories are dis-

cussed. The linearity of climate system responses to different sizes of volcanic eruptions and the carbon cycle-climate sensitivity are determined in section 3b. In sections 3c, 3d and 3e, the focus is on regional changes in the physical, terrestrial and oceanic component and on underlying mechanisms. Then, the long-term impact of historical eruptions on future projections is analyzed in section 3f. A discussion and conclusions are presented in section 4.

## 2 Methods

### 2.1 The NCAR CSM1.4-carbon model

Simulations are performed with the Climate System Model of the National Centre for Atmospheric Research (NCAR CSM1.4-carbon) (Doney et al., 2006; Fung et al., 2005). Atmospheric CO<sub>2</sub> is treated as a prognostic variable whose balance is determined by exchange fluxes with the land and ocean.

The land carbon module combines the NCAR Land Surface Model with a modified version of the terrestrial biogeochemical Carnegie-Ames-Stanford Approach (CASA; Randerson et al. (1997)) providing full coupling of energy (via dynamic leaf phenology and hence albedo), water (via transpiration), and carbon cycles of the atmosphere and land. CASA follows the life cycles of plant functional types from carbon assimilation via photosynthesis, to mortality and decomposition, and the return of CO<sub>2</sub> to the atmosphere via respiration. Autotrophic respiration is not explicitly modeled. Net Primary Production (NPP) is assumed to be 50% of gross primary production. NPP is allocated to three live vegetation pools (leaf, root, and wood) with preferred allocation to roots during water-limited conditions and to wood/leaves during light-limited conditions (Friedlingstein et al., 1999). There are nine soil carbon pools. The transfer rates between them are sensitive to climate and are determined by soil temperature and soil moisture saturation. A fraction of each carbon transfer is released to the atmosphere via microbial or heterotrophic respiration ( $R_h$ ). The land model does not include other land surface processes that affect atmosphere-biosphere interactions such as an explicit nitrogen cycle, fires and other disturbances, herbivory, dynamic vegetation cover, or anthropogenic land cover

change. Changes in diffuse light fraction after a volcanic eruption have no impact on NPP.

Biogeochemistry in the ocean is simulated with a prognostic version (Doney et al., 2006) of the OCMIP-2 biogeochemistry model (Najjar et al., 2007). Prognostic variables in the ocean include phosphate, dissolved inorganic carbon, alkalinity, oxygen, and dissolved organic phosphorus. The marine iron cycle is parametrized and constant Redfield ratios are used.

The radiative volcanic forcing caused by the release of sulphate aerosol into the stratosphere is calculated in the model by prescribing zonal-mean time series of aerosol optical depth (Ammann et al., 2003). The aerosol optical depth was scaled linearly with the aerosol loading assuming a single aerosol distribution of  $0.5 \mu\text{m}$  for volcanic aerosols. Details are described in Ammann et al. (2003). For illustration, the latitudinal distribution of the prescribed aerosol optical depth changes for the Pin.10x case is shown in Fig. 1a. Other factors such as ash, dust, and smoke which have very short lifetimes in the atmosphere are not included. We also neglect any potential direct release of  $\text{CO}_2$  from geological reservoirs. The influx of volcanic bio-available iron in ocean surface waters providing an external nutrient source for primary production is not simulated.

The equilibrium climate sensitivity of the CSM1.4-carbon ( $2^\circ\text{C}$  for a nominal doubling of atmospheric  $\text{CO}_2$ ) is at the lower end of the estimated range of  $2\text{-}4.5^\circ\text{C}$  (Meehl et al., 2007). A significant positive phase of the NAO and the associated winter warming in continental interior of Europe has been found in observations over the last half millennium after volcanic eruptions (Shindell et al., 2004) and is often used to evaluate the volcanic responses in climate simulations (Stenchikov et al., 2006). Encouragingly, the NCAR model shows a tendency to a positive phase of the NAO in pressure and increased temperatures over Eurasia in the first winter after a major low-latitude volcanic eruption. The CSM1.4-carbon physical and biogeochemical climatological mean states are broadly consistent with global ocean and land observations (Doney et al., 2006; Frölicher and Joos, 2010; Frölicher et al., 2009; Fung et al., 2005; Steinacher et al., 2009, 2010). However, there are known biases such as cold anomalies in the surface air temperature over the continental interior in the Northern Hemisphere, precipitation anomalies in the tropics such as the formation of the Intertropical Convergence Zone (ITCZ) over the Pacific as two bands of excess precipitation (the so-called double-ITCZ), and too much or too little

precipitation over land in some tropical regions of South America, Central Africa and South-eastern Asia. These biases in the physical climate also lead to corresponding biases of NPP and carbon storage on land, e.g. an underestimation of NPP in higher latitudes and an overestimation of NPP in lower latitudes. Overall, global NPP resembles reconstructed preindustrial levels (Doney et al., 2006).

## 2.2 Experimental design

Two sets of sensitivity simulations are conducted with the NCAR CSM1.4-carbon (Table 1), all starting from a 1000-yr quasi-stable preindustrial control simulation (Doney et al., 2006) and using the same initial conditions. The variability of a 280-yr control simulation, an extension of the 1000-yr control simulation and performed on the same supercomputer as the sensitivity simulations, is used to determine the statistical significance of the responses.

First, a series of seven model simulations with volcanic eruptions of different strengths are performed over a period of 20 years. The volcanic eruption starts in month six for all cases. These 'scaling experiments' are designed to investigate the response of the coupled carbon cycle-climate system to increasing strength of volcanic perturbations. For the smallest eruption case (Pin.1x) the distribution of aerosol optical depth changes is identical to that of the Mt Pinatubo eruption as given by Ammann et al. (2003). For the other experiments, the aerosol optical depth is scaled by a factor of 2 (Pin.2x), 5 (Pin.5x), 10 (Pin.10x), 20 (Pin.20x), 50 (Pin.50x) and 100 (Pin.100x). The largest simulated eruption (Pin.100x) may be comparable to the Toba eruption (~74 thousand years before present). The Toba eruption is the largest known eruption of the past 100'000 years and could potentially have contributed to glacial cold conditions. One simulation was run for each of these scaling experiments as the size of the climate forcing is likely to produce a response with large signal-to-noise ratio.

Second, two transient simulations with and without historical volcanic forcing are conducted over the period 1820 to 2099. These 'transient experiments' are designed to analyze the long-term impact of volcanic eruptions and to investigate whether it is necessary to include volcanic eruptions in transient simulations over the historical period and future. The non-CO<sub>2</sub> GHG's, sulphate aerosols, and solar irradiance variations are prescribed according to Frölicher et al.

(2009).

To calculate the carbon cycle-climate sensitivity for the industrial period and for the 21st century, we use a simulation with warming and a simulation without warming conducted with the same NCAR CSM1.4-carbon model. Both simulations are forced with historical emissions over the industrial period followed by the SRES A2 IPCC emission scenario. In the simulation without warming, greenhouse gases and other radiative agents were kept at their preindustrial values in the radiation module of the model. For further details see Frölicher et al. (2009) and Frölicher and Joos (2010).

### 2.3 Analysis methods

The focus in the entire manuscript is on the Pin.10x case. It should be viewed as an illustrative example with a reasonably high signal-to-noise ratio. Regional responses after the eruption (apart from the magnitudes) and mechanisms are not fundamentally different in other cases. Unless otherwise noted, the mean annual cycle deduced from the first 20 years of the control simulation has first been removed from the scaling experiments prior to the analysis. The statistical significance of the changes are calculated using two-sided Student's t-test ( $p$  value  $< 0.05$ ).

Different approaches are currently used in literature to estimate the carbon cycle-climate sensitivity  $\gamma$ . The most widely applied are briefly summarized to put the approach adopted here in the context of published studies. Dufresne et al. (2002), Friedlingstein et al. (2006) and Plattner et al. (2008) estimate the climate sensitivity of the land and ocean carbon inventories using a linear feedback approach. Friedlingstein et al. (2006) assume in their equations 2 and 3 that the carbon uptake by land,  $\Delta C_{land}$ , and ocean,  $\Delta C_{ocean}$ , can be approximated by a term which is linear in the change of the global mean atmospheric  $\text{CO}_2$  concentration,  $\Delta C_{atm}$ , plus a term which is linear in the change of global mean atmospheric surface temperature,  $\Delta T$ :

$$\Delta C_{land} + \Delta C_{ocean} = (\beta_{land} + \beta_{ocean}) \cdot \Delta C_{atm} + (\gamma_{land} + \gamma_{ocean}) \cdot \Delta T. \quad (1)$$

$\beta_{land}$  and  $\beta_{ocean}$  denote the sensitivities of land and ocean carbon storage to  $\text{CO}_2$  in GtC per ppm.  $\gamma_{land}$  and  $\gamma_{ocean}$  denote the sensitivities to climate change in units of GtC per  $^\circ\text{C}$ . Together with the mass balance of the volcanic only simulations:

$$\Delta C_{\text{atm}} \cdot 2.123 \text{ GtC ppm}^{-1} + \Delta C_{\text{land}} + \Delta C_{\text{ocean}} = 0, \quad (2)$$

5

equation 1 can be combined to read:

$$\gamma_{\text{land}} + \gamma_{\text{ocean}} = -\frac{\Delta C_{\text{atm}}}{\Delta T} \cdot (2.123 \text{ GtC ppm}^{-1} + \beta_{\text{land}} + \beta_{\text{ocean}}). \quad (3)$$

10

Adapting this approach for our volcano experiments would require a radiatively uncoupled simulation (aerosols and  $\text{CO}_2$  do not influence radiation) with  $\text{CO}_2$  prescribed from the fully coupled simulation to estimate  $\beta$ 's. The approach by [Dufresne et al. \(2002\)](#) and [Friedlingstein et al. \(2006\)](#) is specifically tailored for 21st century simulations with a dominant influence of anthropogenic carbon emissions on the atmospheric  $\text{CO}_2$  increase. However, the approach cannot be readily applied to estimate the  $\text{CO}_2$ -climate sensitivity from observations or proxy reconstructions as the  $\beta$  factors cannot be easily derived from observational data within the required precision.

15

[Scheffer et al. \(2006\)](#), [Frank et al. \(2010\)](#) and [Joos and Prentice \(2004\)](#) used an alternative approach to exploit information from the last millennium paleo-records of atmospheric  $\text{CO}_2$  and temperature. They estimate the sensitivity as regression or ratio between changes in atmospheric  $\text{CO}_2$  and temperature (termed  $\alpha$  in [Scheffer et al. \(2006\)](#) and  $\gamma$  in [Frank et al. \(2010\)](#)) as:

20

$$\gamma_{\text{Frank}} = \alpha_{\text{Scheffer}} = \frac{\Delta C_{\text{atm}}}{\Delta T}. \quad (4)$$

This approach is suitable to estimate the sensitivity directly from the CO<sub>2</sub> and temperature records. Here, we followed this second, observation-based approach. However, a regression as applied in the studies by Scheffer et al. (2006) and Frank et al. (2010) is not meaningful in the context of our volcanic simulations as the evolution of CO<sub>2</sub> and temperature is different on the multi-annual time scales of the simulations. Instead, we average the signals over time and estimate  $\gamma$  as the ratio between the temporal global mean atmospheric CO<sub>2</sub> change and the temporal global mean atmospheric surface temperature change:

$$\gamma_{\text{this study}} = \frac{\overline{\Delta C_{\text{atm}}}}{\overline{\Delta T}}. \quad (5)$$

The above equation is evaluated for different averaging periods: 5, 10, 15, 20 yr after the eruption. We also computed sensitivities estimates using peak values ( $\gamma = \Delta C_{\text{atm,peak}} / \Delta T_{\text{peak}}$ ), but this does not alter our conclusions (not shown).

$\gamma$  is also computed from our CSM1.4 simulations over the industrial period and the 21st century consistent with the above approach. In detail,  $\gamma$  are obtained by calculating temperature and CO<sub>2</sub> differences between a simulation with warming and a simulation without warming and estimating the regression of residual time-series. The temperature and CO<sub>2</sub> differences have first been smoothed with a 10-yr running mean before calculating regression coefficients (Roy et al., 2011), as we are interested in isolating the long-term trends in CO<sub>2</sub> storage for this century scale simulations.

Changes in Dissolved Inorganic Carbon (DIC) are investigated as salinity-normalized changes ( $s\text{DIC} = \text{DIC} * 34.73/S$ ).  $s\text{DIC}$  is not affected by freshwater flux changes. Following Plattner et al. (2008) and Frölicher et al. (2009), the changes in  $s\text{DIC}$  are attributed to changes in the marine biological cycle,  $\Delta s\text{DIC}_{\text{bio}}$  and to residual changes,  $\Delta s\text{DIC}_{\text{res}}$ . The volcanic induced cooling reorganizes the marine organic matter cycle and the calcite cycle. This reorganization

is driven by changes in circulation and water mass distribution and changes in productivity and export of organic matter and calcite. The latter are related to changes in physical parameters and nutrient availability. Changes in DIC related to changes in marine productivity and remineralization of organic matter and calcite are linearly linked to changes in phosphate ( $\Delta\text{PO}_4$ ) and alkalinity ( $\Delta\text{ALK}$ ) by Redfield ratios in the NCAR CSM1.4-carbon. This allows us to quantify the local effect of this reorganization on DIC as:

$$\Delta\text{sDIC}_{\text{bio}} = 117 \cdot \Delta\text{PO}_4 + 0.5 \cdot (\Delta\text{sALK} + 16 \cdot \Delta\text{PO}_4). \quad (6)$$

The first term on the right hand side of the equation represents the reorganization of the organic matter cycle with the carbon-to-phosphate Redfield ratio of 117. The second term represents the reorganization of the calcite cycle as obtained from simulated changes in alkalinity and phosphate with the alkalinity-to-phosphate Redfield ratio of 16, and with the carbon-to-alkalinity ratio of  $\text{CaCO}_3$  of 0.5. The whole ocean inventory of  $\Delta\text{sDIC}_{\text{bio}}$  is conserved. In contrast, changes in residual DIC ( $\Delta\text{sDIC}_{\text{res}} = \Delta\text{sDIC} - \Delta\text{sDIC}_{\text{bio}}$ ) reflect altered air-sea fluxes. Changes in air-sea gas exchange result from a variety of processes such as changes in solubility e.g. related to cooling, and changes in surface ocean DIC and ALK concentration in response to ventilation changes and altered nutrient cycling.

### 3 Results

#### 3.1 Global mean changes

In general, the magnitude of climate and carbon cycle responses and the time scales of recovery increase with the strength of volcanic perturbations (Fig. 1). Aerosol optical depth increases to a maximum within the first 5 months after the eruption and gradually returns to its background

level over the next several years (Fig. 1a). A maximum reduction in global mean net solar radiation of  $37 \text{ W m}^{-2}$  (-21%) at the surface is simulated for the Pin.10x case (Fig. 1b). Atmospheric surface temperature drops in all cases within the first months after an eruption, e.g. by  $2.4^\circ\text{C}$  within the two years after the Pin.10x eruption (Fig. 1c). Atmospheric surface temperature recovers on a multi-year to decadal time scale to pre-eruption level. For strong volcanic eruptions, like the Pin.10x case, there is still a significant reduction of temperature after a decade compared to the control simulation. The magnitude of cooling and the recovery time scales additionally depend on the climate sensitivity of the model, which is low in the NCAR model. A stronger cooling and a longer lasting recovery are expected with higher climate sensitivity (Wigley, 2005).

Large volcanic eruptions apparently amplify the seasonal cycle of temperature in the model. Such amplification is illustrated by the wiggles in the evolution of the monthly deseasonalized anomalies in global mean surface temperature (Fig. 1c). A further analysis of this change in seasonality is beyond the scope of this paper.

Atmospheric  $\text{CO}_2$  decreases after a volcanic eruption and shows a delayed response compared to temperature (Fig. 1d). The decrease is up to 8.3 ppm in the Pin.10x case within the first 40 months after the eruption and the atmospheric  $\text{CO}_2$  is still significantly lower than in the control at the end of the simulation. Interestingly, atmospheric  $\text{CO}_2$  and even more land and ocean carbon inventories remain perturbed even in the Pin.1x case after 20 years. The time until the peak in the  $\text{CO}_2$  response is reached increases with the strength of the eruption. The recovery of the atmospheric  $\text{CO}_2$  concentration takes longer than for the bulk change in temperature as longer time scales are involved in the biogeochemical mechanisms than in the physical processes of the atmosphere and the surface ocean (Frölicher and Joos, 2010).

The decadal-scale negative perturbation in atmospheric  $\text{CO}_2$  cause radiative forcing anomalies which influences the temperature evolution. This is superimposed to the short-lived radiative perturbation by sulphate aerosols. To accurately quantify the additional radiative forcing, additional uncoupled simulations with fixed  $\text{CO}_2$  ( $\text{CO}_2$  has no radiative effect) prescribed from the coupled volcanic simulation, would be necessary. The temperature difference between the new experiments and the performed experiments would yield the climate impact of the  $\text{CO}_2$  per-

turbation. However, as a first guess, a 2 ppm decrease as simulated at the end of the simulation in the Pin.10x case gives a radiative forcing of  $-0.15 \text{ W m}^{-2}$  ( $5.35 \text{ W m}^{-2} \cdot \ln(284 \text{ ppm}/282 \text{ ppm})$ ) and an equilibrium global mean surface temperature change of  $-0.02^\circ\text{C}$  ( $0.04 \text{ W m}^{-2} \cdot 2^\circ\text{C} \cdot (3.7 \text{ W m}^{-2})^{-1}$ ) when applying the climate sensitivity of the NCAR model. This is very small, but consecutive eruptions have the potential to leave an integrated signal in the ocean as found in earlier studies (Church et al., 2005; Frölicher et al., 2009; Stenchikov et al., 2009) and further discussed below.

The negative perturbation in atmospheric  $\text{CO}_2$  is mainly driven by an uptake of carbon by the land biosphere (Fig. 1e) and a temporary increase in the ocean carbon inventory (Fig. 1f). The carbon inventory on land remains elevated until the end of the simulation as overturning time scales of carbon in soils range from years to centuries. Interestingly, atmospheric  $\text{CO}_2$  increases and the land carbon inventory decreases in the first couple of years in the Pin.100x. In contrast to the land biosphere, the perturbation in the ocean carbon inventory changes sign for all cases (Fig. 1f). The initial increase in ocean carbon uptake can be explained by an increased solubility of  $\text{CO}_2$  in cooler ocean water (see section 3.5). The ocean changes from a carbon sink to a carbon source after a couple of years because of the large terrestrial carbon uptake and decreasing  $\text{pCO}_2$  in the atmosphere. Therefore, the magnitude of the atmospheric response is mainly determined by the land biosphere while its duration depends on land and ocean processes.

In conclusion, carbon reservoirs and physical variables respond significantly to explosive volcanic eruptions on global scales. The magnitude of changes after large eruptions clearly exceeds internal variability and depends on the strength of the eruptions. Although the net solar radiative flux rapidly returns to its initial value, atmospheric surface temperature and atmospheric  $\text{CO}_2$  concentration remain perturbed over several years or even decades. Thus, very large volcanic eruptions produce small additional radiative forcing through lowered  $\text{CO}_2$ , which perturb the Earth System on longer time scales than the pure atmospheric residence time of the volcanic aerosols.

### 3.2 Carbon cycle-climate sensitivity

The carbon cycle-climate sensitivity  $\gamma$  depend on the time scale considered, on the magnitude of the perturbation, and on the temporal evolution of the perturbation, e.g. exponentially increasing versus pulse-like. Understanding such dependencies is of importance when estimating  $\gamma$  from observations (e.g., Frank et al., 2010; Scheffer et al., 2006; Joos and Prentice, 2004), and from models (e.g., Friedlingstein et al., 2006; Plattner et al., 2008). Here, we combine model estimates of  $\gamma$  from the set of volcanic perturbation experiments with estimates from previously published simulations over the industrial period and the 21st century (Frölicher et al., 2009; Frölicher and Joos, 2010). We consider different averaging periods in the analysis as observational records are typically low-pass filtered prior to the estimation of  $\gamma$ .

In a first attempt, the scaling of the peak perturbations of the climate and carbon cycle is assessed with respect to the volcanic strength (Fig. 2). There is a non-linear relationship between the peak perturbations in global mean surface temperature and atmospheric CO<sub>2</sub> and the perturbation in global mean net surface solar forcing (solid lines in Fig. 2a). The temperature perturbation per unit change in solar flux increases with the magnitude of the eruption, whereas the sensitivity of atmospheric CO<sub>2</sub> to changes in solar flux becomes smaller with increasing eruption strength (Fig. 2a). This difference in sensitivity between temperature and CO<sub>2</sub> has implications for  $\gamma$  as discussed below. As expected from the Beer-Lambert law, global mean shortwave surface radiation does not linearly scale with visible optical depth and the global perturbations in surface temperature and CO<sub>2</sub> scale with the log of the VOD perturbation (dashed lines in Fig. 2a).

The land carbon inventory change per unit change in solar flux decreases with increased strength of the eruption (Fig. 2b). The ocean carbon inventory change scales almost linearly with net surface solar flux change. Thus, the ratio between land carbon uptake and ocean carbon uptake decreases with increasing perturbation strength, from 9.6 for the Pin.2x case to 3.6 for the Pin.100x case (Fig. 2c). Therefore, the impact of the ocean in regulating the magnitude of the atmospheric CO<sub>2</sub> change increases with increasing volcanic strength. However, the land reservoirs remain the major carbon sink after a volcanic eruption in all cases.

Next, the carbon cycle-climate sensitivity  $\gamma$  is computed from the volcanic perturbation simulations and for different time scales applying different time filters by computing the ratio between the temporal mean atmospheric CO<sub>2</sub> and temperature changes (see section 2.3 and Fig. 3,4). The carbon cycle-climate sensitivity ranges from 1.3 ppm/°C for the Pin.100x case and considering a 5-year time period to 33.4 ppm/°C for the Pin.1x case and considering a 20-year time period (Fig. 3b,4). Two distinct features become evident. First,  $\gamma$  increases with increasing time period for all scaling experiments. This is readily explained by the different life time of the temperature and CO<sub>2</sub> perturbations (Fig. 1c,d,3a). The CO<sub>2</sub> perturbation is long-lived, whereas most of the temperature perturbation decays away within the first decade after the eruption. Longer time scales thus imply a much stronger dampening of the temperature signal than of the CO<sub>2</sub> signal. Second,  $\gamma$  decreases with increasing size of the volcanic perturbation. This is explained by the different change in temperature and CO<sub>2</sub> with increasing perturbation size (Fig. 2a) as discussed above. Finally, it should be noted that the signal-to-noise ratio is low for the Pin.1x and Pin.2x cases with long time scales rendering numerical values for these cases statistically uncertain.

In contrast to the pulse-like volcanic perturbations the anthropogenic climate perturbation shows a nearly exponentially growth. This different perturbation characteristic clearly has an impact on  $\gamma$ . The carbon cycle - climate sensitivity which is derived from transient simulations with anthropogenic forcing (SRES A2) using the same model is 4.3 and 9.9 ppm/°C for the historical period and for the 21st century, respectively (Fig. 3b). Thus, as noted earlier,  $\gamma$  is higher for the 21st century where total radiative forcing and climate change is larger than during the industrial period. The estimate of  $\gamma = 6.3$  ppm/°C for the same model in Frank et al. (2010) is consistent with our estimates. They calculated  $\gamma$  for variations in temperature of 0.7°C, typical for the Little Ice Age - modern amplitude. This would correspond to the period 1820 to 2036 in the CSM1.4-carbon model (see Table S3 in Frank et al. (2010)); note that the period is not correctly given in Frank et al. (2010): 1861 to 2077 instead 1820 to 2036) and lies between our estimate for the period 1820 to 1999 and the period 2000 to 2099. Plattner et al. (2008) find that  $\gamma$  only weakly depends on the choice of the 21st century scenario in their transient simulations.

In conclusion, the carbon cycle-climate sensitivity differs between pulse-like volcanic perturbations and global warming simulations. For the pulse-like perturbations,  $\gamma$  decreases with eruption size and the magnitude of the radiative forcing and increases when evaluated over longer time period. For the SRES A2 business-as-usual scenario,  $\gamma$  becomes larger with time and increasing magnitude of radiative forcing and climate change. Finally,  $\gamma$  is considerably larger for a Pinatubo-like eruption than for simulations over the industrial period and the 21st century in the NCAR CSM1.4.

### 3.3 Regional changes in the physical climate system

Net surface solar flux, temperature, precipitation, and soil moisture plays a major role in controlling the carbon cycle on the regional scale. To illustrate regional changes in these variables due to volcanic eruptions, we show difference patterns between the Pin.10x case and the control simulation averaged over the first 5 years (Fig. 5).

The prescribed aerosol optical depth changes are not uniformly distributed (Fig. 1a) and the net surface solar flux is mainly decreased in low and mid-latitudes ( $50^{\circ}\text{N}$  to  $40^{\circ}\text{S}$ , Fig. 5a). The difference pattern of temperature (Fig. 5b) exhibits a strong cooling over the continents and in the Arctic and small changes or even some warming over the Southern Ocean. Greenland, Alaska and parts of North India experience the largest temperature anomalies with values of less than  $-3^{\circ}\text{C}$ , whilst Europe and the northern part of Asia show a much smaller cooling or even a slight warming. This is due to the short-term dynamical changes in the troposphere-stratosphere system in these regions (Shindell et al., 2004).

Global mean precipitation is reduced by up to  $0.5 \text{ mm d}^{-1}$  (17%) in the first 5 years parallel to global mean atmospheric surface temperature in the Pin.10x case compared to the control simulation. On regional scale, precipitation reduction exceeds natural variability in many tropical and mid-latitude regions, such as Indonesia, the northern part of South America, the western part of North America and central Europe, and over the tropical Pacific Ocean in the latitudinal bands around  $20^{\circ}\text{N}$  to  $5^{\circ}\text{N}$  and  $5^{\circ}\text{S}$  to  $20^{\circ}\text{S}$  (Fig. 5c), and parts of the Southern Ocean around  $40^{\circ}\text{S}$  to  $50^{\circ}\text{S}$ . Precipitation is increased in some regions, e.g. around the equator in the tropical Pacific and Indian Ocean. This could be traced back to model biases (double ITCZ). Still, in

most regions the difference pattern of precipitation is not significant; this holds also for the analysis of seasonal precipitation changes. Our results for the Indian subcontinent are in contrast to those of [Robock et al. \(2008\)](#). These authors conclude that maintained artificial injections of sulfate aerosols to mitigate global warming would suppress water supply in the region of India.

5 In our model and for a pulse-like sulfur injection, the decrease in precipitation is not significant, although the simulated precipitation changes are in general similar to those of [Robock et al. \(2008\)](#).

Changes in soil moisture represent the difference in precipitation and evapotranspiration. The latter depends on physical and biological mechanisms. Consequently, the perturbations  
10 in soil moisture do not scale simply with precipitation changes. Drier soils are simulated in northern mid-latitudes and northwestern South America, and soil moisture is increased around the Mediterranean Sea, in Southern Asia, in the southwestern part of North America and in northeastern South America (Fig. 5d).

In conclusion, the difference patterns show that the temperature changes on the Earth surface  
15 as a consequence of volcanic eruptions has been qualitatively successfully simulated in comparison with data-based reconstructions ([Robock and Mao, 1992](#)). Interestingly, some grid cells show no significant cooling even for the Pin.10x case. Furthermore, the simulated precipitation anomalies are highly uncertain and depend on the model as shown by comparison with the results of [Robock et al. \(2008\)](#).

### 20 **3.4 Terrestrial biosphere changes and mechanisms**

As illustrated in Fig. 1e the land carbon inventory increases after a volcanic eruption. The time-integrated response of the land carbon inventory to the Pin.10x eruption is divided into soil and vegetation carbon pools as well as into Net Ecosystem Production (NEP), net primary production and heterotrophic respiration (Fig. 6a). Most of the carbon is taken up by the  
25 soil carbon pools within the first 5 years after the eruption, while the vegetation pools (mainly wood allocation) and time-integrated NPP slightly decrease in the first decade. Both soil and vegetation carbon pools remains perturbed by the end of the simulation. NEP changes result from differing sensitivities of vegetation and soil carbon pools to changes in light, temperature,

precipitation, and soil moisture (Fig. 5). The net effect on NEP depends on their synergistic or competing effects.

On regional scales, the increase in NEP occurs mainly in the tropics as illustrated for the Pin.10x case in Fig. 6b. The total carbon storage in soil and vegetation is increased in most of the tropical regions; changes elsewhere are small. Vegetation carbon changes in the tropics (Fig. 6c,f) are opposite in regions with negative soil moisture changes (and negative precipitation anomalies) and in regions with small and positive soil moisture changes (Fig. 5c,d). Drying and soil moisture decrease lead to a decrease in NPP in northwestern South America, in parts of East Africa and in Indonesia, and thus to a decrease in vegetation carbon pools (Fig. 6c,f). A significant connection between soil moisture and NPP is simulated in these regions as the regression pattern in Fig. 7a shows. Besides soil moisture decrease (Fig. 7b), volcanic-induced cooling causes soil temperature and soil overturning rates to decrease (Fig. 7d). The decrease in soil overturning and associated increase in soil carbon (Fig. 6e) overcompensates the decrease in litter flux (carbon flux from vegetation pools to soil pools) due to the NPP decrease, resulting in higher soil carbon inventories.

In tropical regions (e.g. Northeast South America) where small or positive soil moisture changes are simulated after the volcanic eruption, the NPP and the vegetation carbon pool increase due to the volcanic-induced cooling. In contrast to the drying regions discussed above, cooling leads to an increase in NPP at these locations. These are regions where NPP and temperature changes are strongly related in the tropics (Fig. 7c). Soil overturning rates are also reduced, which leads to an increase in soil carbon content. Thus, soil and vegetation carbon pools increase in regions with a positive soil moisture perturbation.

In mid-latitudes of North America and Europe, cooling and soil moisture changes lead to a decrease in NPP (Fig. 7a,c) and vegetation carbon pools, and thus to a decrease in litter flux. The cooling also reduces the soil overturning rates (Fig. 7d) and increases soil carbon content. This effect dominates over reduced litter input. Totally, NEP changes are about zero, as vegetation carbon changes and soil carbon changes compensate each other.

In the Pin.10x case the direct radiative decrease plays a minor role in controlling NPP in the tropics. However, light-limitation could play a role for very strong volcanic eruptions (e.g.

Pin.100x case) in mid-latitudes (not shown).

Heterotrophic respiration decreases in many regions, worldwide (Fig. 6d). The largest reductions in  $R_h$  are simulated in tropical South America, Africa and Indonesia as well as in northern mid-latitudes, whereas small increases in  $R_h$  are simulated in northern subtropical regions. Overall, the interpretation of  $R_h$  changes is complicated by different influencing factors and processes with very different time scales.  $R_h$  changes depend on NPP and vegetation carbon turnover through their influence on litter flux as well as on changes in the turnover rates of soil and litter carbon and thus on temperature and soil moisture changes. A full detailed analysis of changes in respiration is beyond the scope of the manuscript.

In conclusion, the tropical terrestrial biosphere is sensitive to low-latitude volcanic eruptions and perturbations last up to several decades. Changes in NPP and vegetation carbon are strongly influenced by changes in soil moisture which vary across regions. Soil moisture changes have a stronger impact on NPP than on heterotrophic respiration in this model. Changes in soil carbon are dominated by reduced soil turnover rates in response to volcanic cooling (and soil moisture changes) in most regions. In mid-latitudes, changes in the vegetation and soil carbon pools compensate each other in the NCAR CSM1.4-carbon, whereas soil carbon changes dominate the response in the tropics.

### 3.5 Ocean carbon and marine biosphere changes and mechanisms

Besides the terrestrial changes the ocean carbon cycle play an important role in regulating atmospheric  $\text{CO}_2$  after explosive volcanic eruptions. We therefore focus on the ocean carbon uptake and release and changes in the oceanic distribution of sDIC and pH at the surface (Fig. 8, 9) and at different depths levels (Fig. 10-12) due to different mechanisms using the Pin.10x case as an archetype.

In the first 5 years after the volcanic eruption, the largest increases in sDIC are simulated in low-latitude shallow waters between  $40^\circ\text{N}$  and  $40^\circ\text{S}$  (Fig. 8a, 10a,b). The increase in sDIC there is mainly caused by an increase in  $\text{sDIC}_{\text{res}}$  (Fig. 8c) due to volcanic-induced cooling (Fig. 5b,8g,10g,h) and an associated increase in the solubility of  $\text{CO}_2$  which enhances air-sea carbon flux (Fig. 8d). Less grid cells for air-sea carbon fluxes are statistically significant than

for  $sDIC_{res}$  changes due to the high variability of air-sea carbon fluxes in the control simulation. The enhanced carbon storage by the ocean in the first years after the eruption are also shown by the positive anomalies in  $sDIC_{res}$  in low-latitude shallow waters in the Atlantic as well as the Indo-Pacific Ocean (Fig. 10e,f). In southern high latitudes between  $40^{\circ}S$  and  $60^{\circ}S$ , decreases in  $sDIC_{bio}$  lead to a decrease in  $sDIC$  there (Fig. 8b,10e,f).

Interestingly, significant increases in pH are simulated almost everywhere (Fig. 9a), although  $sDIC$  and SST do not change uniformly (Fig. 8a,g). In order to quantify the driving mechanisms of the pH changes, we used the unperturbed SST from the control simulation when calculating the pH changes to distinguish the pH changes caused by SST changes alone ( $\Delta pH_{SST}$ ) and pH changes due to other drivers (DIC, ALK, SSS). The pH changes in low latitudes are mainly driven by the decrease in SST (Fig. 9b), somewhat damped by the increase in  $sDIC$  (Fig. 9c, 8a). A reduction of SST leads to changes in the dissociation constants, which change the partitioning of total DIC among the various carbon species. In high latitudes (e.g. between  $40^{\circ}S$  and  $60^{\circ}S$ ) changes in pH are mainly driven by changes in DIC and/or ALK (Fig. 9c, 8a,f). SST changes there are small.

Below 200 meters,  $sDIC$  changes in both basins are caused by reorganizations of the marine biological cycle ( $sDIC_{bio}$ ; Fig. 10c,d), which are associated with decreased stratification and increased deep to surface exchange of nutrients and carbon. Global integrated export of particulate organic carbon increases significantly by 4% ( $0.37 \text{ Gt C yr}^{-1}$ ) averaged over the first 5 years after the Pin.10x eruption. The largest increases in export production are simulated in the North Atlantic region where it increases locally by up to 30 to  $40 \text{ g C m}^{-2} \text{ yr}^{-1}$  (Fig. 8e). In other regions, smaller changes are simulated as is also the case in global warming simulations (Steinacher et al., 2010).

The temporal evolution of zonally averaged  $sDIC$  concentration anomalies in the upper 1500 m of the Atlantic and Indo-Pacific Ocean after the Pin.10x eruption is shown in Fig. 11. The positive  $sDIC$  anomalies penetrate below the surface in both basins during the first years after the eruption (Fig. 11a,b). Also cold surface water are gradually transferred to greater depths (Fig. 11g,h). The persistent positive anomalies in  $sDIC$  in the Atlantic subsurface waters are mainly related to a reorganization of the marine biological cycle (Fig. 11c).

At the end of the Pin.10x simulation, sDIC shows a complex structure in the North Atlantic (Fig. 12a), whereas changes in sDIC in the Indo-Pacific are small (not shown). The changes in sDIC in the North Atlantic are mainly caused by changes in  $sDIC_{bio}$ , which are linked to an increase in the strength and penetration of the Atlantic Meridional Overturning Circulation (AMOC; Fig. 12b), decreased stratification and increased surface-to-deep exchange which increase penetration of nutrients and carbon in shallow waters and in turn productivity and export production. The AMOC is enhanced by up to 5 Sv for the Pin.10x case. As the AMOC has inherent decadal time scales of adjustment (Delworth and Dixon, 2006), large changes in sDIC are simulated one to two decades after the volcanic eruption.

The carbon balance of the Atlantic as well as the Pacific Ocean becomes negative around 5 years after the volcanic eruption as evidenced by negative anomalies in  $\Delta sDIC_{res}$  (Fig. 11e,f). The loss of carbon is caused by lower  $pCO_2$  concentration in the atmosphere than in the ocean because of the large terrestrial carbon uptake (also seen in Fig. 1f).

In conclusion, a significant reorganization in DIC occurs, mainly in the North Atlantic Ocean. Although the ocean loses carbon after 5 years, positive DIC anomalies in the thermocline last up to several decades in the Atlantic Ocean.

### 3.6 Long-term impact of historical volcanic eruptions

As shown above, volcanic eruptions have the potential to generate considerable variability in the biogeochemical system and the perturbation persists for several decades. This poses the question whether transient projections over the historical period and for the next century depend on the treatment of volcanic eruptions. Only 14 out of 23 fully coupled models used for the IPCC fourth Assessment Report (AR4) have implemented volcanic eruptions over the historical period and none has included possible future eruptions (Meehl et al., 2007).

To investigate the long-term impact of volcanic eruptions transient experiments have been conducted (Table 1). Fig. 13 shows times-series of differences from simulations with and without historical volcanic forcing over the period 1820 to 2099 for different atmospheric and oceanic properties. Historical eruptions exert a small influence on projected atmospheric surface temperature, atmospheric  $CO_2$  and global land and ocean carbon inventory in comparison with

the substantial internal, multi-decadal variability (Fig. 13a,d-f). This small impact may be explained by the low climate sensitivity and the low climate-carbon cycle sensitivity  $\gamma$  of the NCAR CSM1.4-carbon and that only few eruptions are of comparable or larger magnitude than the Pinatubo eruption. In contrast, volcanic induced changes in ocean quantities such as potential temperature, steric sea level and ocean oxygen inventory last well into the 21st century. The abrupt changes in steric sea level (Fig. 13b) and dissolved oxygen (Fig. 13c) are associated with major volcanic eruptions. Historical volcanic eruptions reduce the secular increase in potential temperature by 8.4% (0.03°C) in year 2099 (not shown). Accordingly, the global steric sea level rise is damped by 7.6% (1.5 cm) in year 2099 if historical volcanic eruptions are included. The O<sub>2</sub> increase due to historical volcanic eruptions offsets 11% (0.6 Pmol) of the negative trend in O<sub>2</sub> in year 2099 caused by global warming due to anthropogenic forcing. The initial increase in dissolved oxygen inventory (0.5 Pmol) over the period 1820 to 1920 in transient ensemble simulations with the same model (c.f. Fig. 2a in Frölicher et al. (2009)) can thus be explained by volcanic eruptions. The ocean carbon inventory, on the other hand, is hardly affected on a global scale (Fig. 13f), but a slight redistribution of carbon in the ocean is simulated for the future. More DIC in the upper ocean and less DIC in the deeper Ocean are projected in year 2099 if volcanic eruptions are included (not shown).

In summary, although historical volcanic eruptions last for 2-3 years in the lower atmosphere, the ocean integrates volcanic radiative cooling and responds over a wide range of time scales for different physical and biogeochemical oceanic parameters.

## 4 Discussion and conclusions

The sensitivity of short- and long-term impacts to the strength of explosive volcanic eruptions on the carbon cycle-climate system on both the global and regional scale is investigated with a comprehensive fully coupled climate-carbon cycle model. In Pinatubo scaling experiments aerosol optical depth is scaled over two orders of magnitude and a non-linear relationship is found between peak changes in net surface solar flux, surface atmospheric temperature and atmospheric CO<sub>2</sub> concentration.

The skill of the NCAR CSM1.4-carbon model in representing climate and carbon and tracer distribution in the land-ocean-atmospheric system is documented in a number of papers (e.g., [Doney et al., 2006](#); [Frölicher et al., 2009](#)). Clearly, some caveats remain from this study. First, by scaling the aerosol optical depth changes of the Pinatubo forcing, any of the non-linear chemical processes responsible for aerosol growth that may occur following a very large volcanic eruption are neglected. [Timmreck et al. \(2010\)](#) showed that the implementation of particle size evolution likely reduces the temperature response after large eruptions. Secondly, the impact on the biological carbon pump by nutrient addition from volcanic ash to the surface ocean is neglected in this study. It has been hypothesized that iron fertilization of the Southern Ocean by volcanic ash from Mt. Pinatubo caused an additional uptake of CO<sub>2</sub> on the order of 1-2 Gt carbon ([Watson, 1997](#)). Although, recent laboratory experiments and direct evidence in the North Pacific Ocean indicate that primary production may indeed be affected by volcanic ash supply ([Lin et al., 2011](#); [Duggen et al., 2010](#)), the impact on global atmospheric CO<sub>2</sub> concentration remains unclear ([Hamme et al., 2010](#)). Future research is needed to reduce this uncertainty. Thirdly, the sensitivity of NPP to changes in the ratio of direct to diffuse radiation changes is not included in the NCAR CSM1.4-carbon land model ([Gu et al., 2003](#)). [Mercado et al. \(2009\)](#) suggested in a modeling study that an increase in diffuse radiation after the Mt Pinatubo eruption may have enhanced the terrestrial carbon sink.

Large explosive volcanic eruptions perturb atmospheric CO<sub>2</sub> and biogeochemical cycles for decades. A positive, but small Earth System feedback is identified that amplifies the climate impacts of large explosive volcanic eruptions (Fig. 14). Sulphate aerosols injected into the stratosphere cause a reduction in solar shortwave radiation at the surface. In response, surface land and ocean temperature cool and precipitation pattern changes. Soil overturning rates are reduced and carbon uptake by the land biosphere is enhanced. CO<sub>2</sub> solubility in ocean surface water is increased causing a decrease in surface water pCO<sub>2</sub> and carbon uptake from the atmosphere. This solubility effect on air-sea flux is partly offset by enhanced overturning and mixing leading to higher nutrient and carbon input to the surface. Carbon uptake by the land and ocean causes a reduction in atmospheric CO<sub>2</sub> and a small negative radiative forcing by CO<sub>2</sub>. This amplification is very small for the NCAR CSM1.4-carbon model, but could potentially be larger

in other Earth System Models or in reality.

The simulated changes in land and ocean carbon inventories may be related to estimates of the contemporary carbon sink fluxes into the land and ocean. The net air-to-land carbon flux is estimated as  $10 \pm 6$  GtC and the net air-to-sea flux as  $22 \pm 4$  GtC for the 1990 to 1999 period (Denman et al., 2007). Taken at face value, our results for the Pin.1x case suggest a contribution of about 4 GtC to the terrestrial sink and a small contribution to the ocean sink caused by the Pinatubo eruption (Fig. 1e,f). However, and also in evidence in Fig. 1e, internal variability in land carbon storage is substantial and may contribute to the simulated increase in land storage in the Pin.1x simulation. On the other hand, both the climate and the carbon cycle-climate sensitivity are relatively low in the NCAR CSM1.4 and a higher sensitivity likely implies a higher land uptake as for example found in the Pin.2x or Pin.5x cases. Earlier work also inferred a sustained increase in the terrestrial sink flux in the late 1980s (Joos et al., 1999; Denman et al., 2007; Sarmiento et al., 2010). Denman et al. (2007) estimate an average net atmosphere-to-land flux of  $0.3 \text{ GtC yr}^{-1}$  for the 1980s and of  $1.0$  and  $0.9 \text{ GtC yr}^{-1}$  for the 1990s and the period 2000 to 2005. While detailed analyses show that the increase in flux occurred before the Pinatubo eruption, the Pinatubo effect may have contributed to the large terrestrial sink flux inferred for the last 20 years. Overall, our model results suggest a contribution to the terrestrial sink flux by volcanic eruptions and that the persistence of the additional land carbon storage is multi-decadal.

The finding that land uptake occurs mainly in the tropics is in line with previous studies (Brovkin et al., 2010; Jones and Cox, 2001). They both found that a strong reduction in heterotrophic respiration on land is responsible for the enhanced uptake. Here, we focus more on soil and vegetation carbon pools changes rather than on heterotrophic respiration changes. In NCAR CSM1.4-carbon the terrestrial carbon uptake in the tropics is caused by reduced soil overturning which dominates over reduced litter input due to soil moisture decrease. Compensating effects in the northern mid-latitudes lead to no changes there. A predominant role of tropical changes is also found in other simulations with the NCAR CSM1.4 model including business-as-usual 21st century scenarios (Fung et al., 2005; Frölicher and Joos, 2010) and freshwater release experiments (Bozbyik et al., 2010). However, the near cancellation of opposing

changes in vegetation and soil carbon in extratropical regions for a range of experimental setups is model-dependent (e.g., [Lucht et al., 2002](#)). The initial ocean cooling contributes to the negative atmospheric CO<sub>2</sub> anomaly during the first years after an eruption by stimulating ocean carbon uptake. Afterwards, the ocean tends to mitigate the atmospheric CO<sub>2</sub> perturbation and to release carbon. In contrast to [Brovkin et al. \(2010\)](#) not only the ocean but both the land and the ocean are responsible for the time lag of the maximum CO<sub>2</sub> response.

Our simulations show that the ocean has a long memory effect of volcanic eruptions. The Pinatubo scaling experiments reveal a significant redistribution of the carbon cycle in the North Atlantic, an enhancement of productivity and a strengthening of the Atlantic Meridional Overturning Circulation that persists up to several decades. These results have implications for interpreting current carbon sink estimates in the North Atlantic Ocean. Observational studies suggest that the carbon sink in the North Atlantic has decreased over the past two decades, possibly reflecting the impact of long-term climate change (e.g., [Metzl et al., 2010](#); [Schuster et al., 2009](#); [Pérez et al., 2008](#); [Schuster and Watson, 2007](#)). Given the long-term impact of volcanic eruptions on DIC and air-sea gas exchange, especially in the North Atlantic, the interpretation of long-term trends in the ocean carbon sink should be viewed with caution ([Thomas et al., 2008](#)). As most time-series start in early 1990s the carbon measurements may contain a perturbed signal from Pinatubo. However, further research and comparison of our Pin.1x simulation with continued time-series of  $\Delta p\text{CO}_2$  and carbonate system parameters is needed to make reliable conclusions.

Our simulations show that perturbations of historical eruptions as found by comparing simulations with and without historical volcanic eruptions last well into the 21st century. This is consistent with the findings of [Church et al. \(2005\)](#), [Frölicher et al. \(2009\)](#) and [Stenchikov et al. \(2009\)](#). As only a subset of models used in the IPCC AR4 report includes variable volcanic forcing over the historical period and none includes possible future volcanic eruptions ([Meehl et al., 2007](#)), projections of steric sea level rise and ocean temperature in the AR4 may include a bias. We note that our 1000-yr control simulation spin-up has been equilibrated to preindustrial conditions free of volcanic eruptions, and that this likely induces an initial cooling when volcanic forcing is included ([Gregory, 2010](#)). However, our results regarding the short-term

impacts of volcanic eruptions are not affected by the volcano-free control spin-up.

Our study shows that the carbon cycle-climate sensitivity  $\gamma$  differs between pulse-like volcanic perturbations and near-exponentially increasing anthropogenic forcing and that estimated values depend on the time scales of interest.  $\gamma$  decreases with increasing magnitude of the volcanic perturbation and increases with increasing temporal smoothing of the model output, a feature also found by Frank et al. (2010). Recently, this metric has become the focus of a number of studies on the carbon cycle-climate feedbacks.  $\gamma$  has been computed across a range of models for simulations over the industrial period and business-as-usual scenarios (e.g., Friedlingstein et al., 2006; Dufresne et al., 2002; Plattner et al., 2008) or derived from proxy data (Joos and Prentice, 2004; Scheffer et al., 2006; Frank et al., 2010). Frank et al. (2010) computed  $\gamma$  from temperature and CO<sub>2</sub> records for the last millennium in a probabilistic way applying a range of records, analysis periods and smoothing. Most of the forced climate variations during the last millennium are attributed to volcanic forcing and some to solar forcing (e.g., Ammann et al., 2007; Jansen et al., 2007; Gerber et al., 2003) and this raises the question whether their results apply also for the industrial period and the next century with more or less steadily increasing forcing. Fig. 4 shows that  $\gamma$  obtained from the Pin.5x to Pin.100x scaling experiments varies between 1 and 11 ppm/°C for the different cases and the range of smoothing applied. This is broadly comparable to  $\gamma$  estimated over the historical period (4 ppm/°C) and for the 21st century and the SRES A2 scenario (10 ppm/°C). Note however, that much larger values for  $\gamma$  are obtained for the two smaller scaling experiments, but the statistical uncertainty is large for these two cases due to a small signal compared to internal variability. In brief, the simulated sensitivity of the atmospheric CO<sub>2</sub> concentration to temperature depends on the forcing type, the forcing strength and the time scales of interests. The mechanisms in play might be different for a volcanic eruption than for an exponentially increasing perturbation. This makes a clear comparison of  $\gamma$  derived from proxy data and with model estimates using different forcing types somewhat difficult, although the analysis of the proxy data likely reveals the right order of magnitude of  $\gamma$ . Simulations that directly attempt to model the relationship between volcanic and solar forcing, climate change, and changes in atmospheric CO<sub>2</sub> over the last millennium (Jungclauss et al., 2010; Gerber et al., 2003) and as planned as part of the PMIP

suite of experiments (Schmidt et al., 2011) will hopefully reveal more insights.

A range of potential geoengineering options as a means to limit potential impacts of anthropogenic carbon emissions and climate change are currently being discussed. One of the most prominent geoengineering ideas proposed to counteract global warming today involves increasing Earth's albedo by artificially releasing sulphate aerosols into the stratosphere (Crutzen, 2006; Wigley, 2006; Royal Society, 2009). Thus, volcanic eruptions could be considered as an analog for geoengineering. As has been shown here, enhanced stratospheric sulphate aerosol content can reduce global mean surface temperature, but has only a modest impact on the atmospheric CO<sub>2</sub> rise driven by fossil fuel use. The relatively small enhanced uptake of the land and ocean components (relative to current carbon emission) has no long-lasting counteracting positive effects on the atmospheric CO<sub>2</sub> rise and ongoing ocean acidification (Orr et al., 2005). Other studies of this option have shown that responses in surface temperature and precipitation vary widely across regions and geoengineering with sulphate aerosols or other albedo devices may potentially aggravate climate change problems in certain regions. If the engineered system later fails for technical or policy reasons, the downside is dramatic, as an abrupt warming after termination of stratospheric aerosol loading is expected (Brovkin et al., 2009; Robock et al., 2008).

*Acknowledgements.* Simulations were carried out at the Swiss National Computing Centre in Manno, Switzerland. TLF is supported by the SNSF. CCR is supported the NCCR Climate and the project FUPSOL, both funded by SNSF. We thank JL Sarmiento, KB Rodgers and D Paynter for discussion, and two anonymous reviewers for constructive comments. This work is a contribution to the "European Project on Ocean Acidification" (EPOCA) which received funding from the European Community's Seventh Framework Programme (FP/2007-2013) under grant no. 211384.

## References

Ammann, C. M., Meehl, G. A., Washington, W. M., and Zehnder, C. S.: A monthly and latitudinally varying volcanic forcing dataset in simulations of 20th century climate, *Geophys. Res. Lett.*, 30(12), 1657, doi:10.1029/2003GL016875, 2003. 8, 9

- Ammann, C. M., Joos, F., Schimel, D. S., Otto-Bliesner, B. L., and Tomas, R. A.: Solar influence on climate during the past millennium: Results from transient simulations with the NCAR climate system model, *Proc. Natl. Acad. Sci.*, 104, 3713–3718, doi:10.1073/pnas.0605064, 2007. 4, 28
- Angert, A., Biraud, S., Bonfils, C., Buermann, W., and Fung, I.: CO<sub>2</sub> seasonality indicates origins of post-Pinatubo sink, *Geophys. Res. Lett.*, 31, L11 103, doi:10.1029/2004GL019760, 2004. 5
- Bacastow, R. B., Adams, J. A., Keeling, C. D., Moss, D. J., Whorf, T. P., and Wong, C. S.: Atmospheric carbon dioxide, the Southern Oscillation, and the weak 1975 El Niño, *Science*, 210, 66–68, doi:10.1126/science.210.4465.66, 1980. 3
- Baker, D. F., Law, R. M., Gurney, K. R., Rayner, P., Peylin, P., Denning, A. S., Bousquet, P., Bruhwiler, L., Chen, Y.-H., Ciais, P., Fung, I. Y., Heimann, M., John, J., Maki, T., Maksyutov, S., Masarie, K., Prather, M., Pak, B., Taguchi, S., and Zhu, Z.: TransCom 3 inversion intercomparison: Impact of transport model errors on the interannual variability of regional CO<sub>2</sub> fluxes, 1988–2003, *Global Biogeochem. Cycles*, 20, doi:10.1029/2004GB002439, 2006. 5
- Bousquet, P., Peylin, P., Ciais, C. L. Q., Friedlingstein, P., and Tans, P.: Regional changes in carbon dioxide fluxes of land and oceans since 1980, *Science*, 290, 1342–1346, doi:10.1126/science.290.5495.1342, 2000. 5
- Bozbyk, A., Steinacher, M., Joos, F., and Stocker, T. F.: Fingerprints of changes in the terrestrial carbon cycle in response to large reorganizations in ocean circulation, *Clim. Past Disuss.*, 6, 1811–1852, 2010. 26
- Brovkin, V., Petoukhov, V., Claussen, M., Bauer, E., Archer, D., and Jaeger, C.: Geoengineering climate by stratospheric sulfur injections: Earth system vulnerability to technological failure, *Clim. Change*, 92, 243–259, doi:10.1007/s10584-008-9490-1, 2009. 29
- Brovkin, V., Lorenz, S. J., Jungclaus, J., Raddatz, T., Timmreck, C., Reick, C. H., Segschneider, J., and Six, K.: Sensitivity of a coupled climate-carbon cycle model to large volcanic eruptions during the last millennium, *Tellus B*, 62, 674–681, doi:10.1111/j.1600-0889.2010.00471.x, 2010. 4, 6, 26, 27
- Canadell, J. G., Le Quééré, C., Raupach, M. R., Field, C. B., Buitenhuis, E. T., Ciais, P., Conway, T. J., Gillett, N. P., Houghton, R. A., and Marland, G.: Contributions to accelerating atmospheric CO<sub>2</sub> growth from economic activity, carbon intensity, and efficiency of natural sinks, *Proc. Natl. Acad. Sci.*, 104, 18 866–18 870, doi:10.1073/pnas.0702737104, 2007. 3
- Church, J. A., White, N. J., and Arblaster, J. M.: Significant decadal-scale impact of volcanic eruptions on sea level and ocean heat content, *Nature*, 438, 74–77, doi:10.1038/nature04237, 2005. 15, 27
- Crutzen, P.: Albedo enhancement by stratospheric sulfur injections: A contribution to resolve a policy dilemma?, *Clim. Change*, 77, 211–219, doi:10.1007/s10584-006-9101-y, 2006. 29

Delworth, T. L. and Dixon, K. W.: Have anthropogenic aerosols delayed a greenhouse gas-induced weakening of the North Atlantic thermohaline circulation, *Geophys. Res. Lett.*, 33, doi:10.1029/2005GL024980, 2006. **23**

Delworth, T. L., Ramaswamy, V., and Stenchikov, G. L.: The impact of aerosols on simulated ocean temperature and heat content in the 20th century, *Geophys. Res. Lett.*, 32, doi:10.1029/2005GL024457, 2005. **5**

Denman, K. L., Brasseur, G., Chidthaisong, A., Ciais, P., Cox, P. M., Dickinson, R. E., Hauglustaine, D., Heinze, C., Holland, E., Jacob, D., Lohmann, U., Ramachandran, S., da Silva Dias, P. L., Wofsy, S. C., and Zhang, X.: Couplings between changes in the climate system and biogeochemistry, in: *Climate Change 2007: The Physical Science Basis. Contribution of Working Group I to the Fourth Assessment Report of the Intergovernmental Panel on Climate Change*, edited by Solomon, S., Qin, D., Manning, M., Chen, Z., Marquis, M., Averyt, K., M. Tignor, and Miller, H., pp. 499–587, Cambridge University Press, Cambridge, United Kingdom and New York, NY, USA, 2007. **26**

Domingues, C. M., Church, J. A., White, N. J., Gleckler, P. J., Wijffels, S. E., Barker, P. M., and Dunn, J. R.: Improved estimates of upper-ocean warming and multi-decadal sea-level rise, *Nature*, 453, 1090–1094, doi:10.1038/nature07080, 2008. **5**

Doney, S. C., Lindsay, K., Fung, I., and John, J.: Natural variability in a stable, 1000-yr global coupled climate-carbon cycle simulation, *J. Climate*, 19, 3033–3054, doi:10.1175/JCLI3783.1, 2006. **7, 8, 9, 25**

Dufresne, J.-L., Fairhead, L., Treut, H. L., Berthelot, M., Bopp, L., Ciais, P., Friedlingstein, P., and Monfray, P.: On the magnitude of positive feedback between future climate change and the carbon cycle, *Geophys. Res. Lett.*, 329, doi:10.1029/2001GL013777, 2002. **10, 11, 28**

Duggen, S., Olgun, N., Croot, P., Hoffmann, L., Dietze, H., Delmelle, P., and Teschner, C.: The role of airborne volcanic ash for the surface ocean biogeochemical iron-cycle: a review, *Biogeosciences*, 7, 827–844, doi:10.5194/bg-7-827-2010, 2010. **25**

Frank, D. C., Esper, J., Raible, C. C., Buntgen, U., Trouet, V., Stocker, B., and Joos, F.: Ensemble reconstruction constraints on the global carbon cycle sensitivity to climate, *Nature*, 463, doi:10.1038/nature08769, 2010. **3, 11, 12, 16, 17, 28**

Franklin, B.: Meteorological imaginations and conjectures, *Manchester Literary and Philosophical Society Memoirs and Proceedings*, 2, 1784. **4**

Friedlingstein, P., Joel, G., Field, C. B., and Fung, I. Y.: Toward an allocation scheme for global terrestrial carbon models, *Global Change Biology*, 5, 755–770, doi:10.1046/j.1365-2486.1999.00269.x, 1999. **7**

Friedlingstein, P., Cox, P., Betts, R., Bopp, L., von Bloh, W., Brovkin, V., Cadule, P., Doney, S., Eby,

- M., Fung, I., Bala, G., John, J., Jones, C., Joos, F., Kato, T., Kawamiya, M., Knorr, W., Lindsay, K., Matthews, H. D., Raddatz, T., Rayner, P., Reick, C., Roeckner, E., Schnitzler, K.-G., Schnur, R., Strassmann, K., Weaver, A. J., Yoshikawa, C., and Zeng, N.: Climate-carbon cycle feedback analysis: Results from the C4MIP model intercomparison, *J. Climate*, 19, 3337–3353, doi:10.1175/JCLI3800.1, 2006. [10](#), [11](#), [16](#), [28](#)
- Frölicher, T. L. and Joos, F.: Reversible and irreversible impacts of greenhouse gas emissions in multi-century projections with NCAR global coupled carbon cycle-climate model, *Clim. Dyn.*, 35, 1439–1459, doi:10.1007/s00382-009-0727-0, 2010. [8](#), [10](#), [14](#), [16](#), [26](#)
- Frölicher, T. L., Joos, F., Plattner, G.-K., Steinacher, M., and Doney, S. C.: Natural variability and anthropogenic trends in oceanic oxygen in a coupled carbon cycle-climate model ensemble, *Global Biogeochem. Cycles*, 23, GB1003, doi:10.1029/2008GB003316, 2009. [6](#), [8](#), [9](#), [10](#), [12](#), [15](#), [16](#), [24](#), [25](#), [27](#)
- Fung, I. Y., Doney, S. C., Lindsay, K., and John, J.: Evolution of carbon sinks in a changing climate, *Proc. Natl. Acad. Sci.*, 102(32), 11 201–11 206, doi:10.1073/pnas.0504949102, 2005. [7](#), [8](#), [26](#)
- Gerber, S., Joos, F., Brügger, P. P., Stocker, T. F., Mann, M. E., Sitch, S., and Scholze, M.: Constraining temperature variations over the last millennium by comparing simulated and observed atmospheric CO<sub>2</sub>, *Clim. Dyn.*, 20, 281 – 299, doi:10.1007/s00382-002-0270-8, 2003. [4](#), [5](#), [28](#)
- Gleckler, P. J., AchutaRao, K., Gregory, J. M., Santer, B. D., Taylor, K. E., and Wigley, T. M. L.: Krakatoa lives: The effect of volcanic eruptions on ocean heat content and thermal expansion, *Geophys. Res. Lett.*, 33, L17 702, doi:10.1029/2006GL026771, 2006. [5](#)
- Gloor, M., Sarmiento, J. L., and Gruber, N.: What can be learned about carbon cycle climate feedbacks from the CO<sub>2</sub> airborne fraction?, *Atmos. Chem. Phys.*, 10, 7739–7751, doi:10.5194/acp-10-7739-2010, 2010. [3](#)
- Gregory, J. M.: Long-term effect of volcanic forcing on ocean heat content, *Geophys. Res. Lett.*, 37, L22 701, doi:10.1029/2010GL045507, 2010. [27](#)
- Gu, L., Baldocchi, D. D., Wofsy, S. C., Munger, J. W., Michalsky, J. J., Urbanski, S. P., and Boden, T. A.: Response of a deciduous forest to the Mt. Pinatubo eruption: Enhanced photosynthesis, *Science*, 299, 2035–2038, doi:10.1126/science.1078366, 2003. [25](#)
- Hamme, R. C., Webley, P. W., Crawford, W. R., Whitney, F. A., DeGrandpre, M. D., Emerson, S., Eriksen, C. C., Giesbrecht, K. E., Gower, J. F. R., Kavanaugh, M. T., Pena, M. A., Sabine, C. L., Batten, S. D., Coogan, L. A., Grundle, D. S., and Lockwood, D.: Volcanic ash fuels anomalous plankton bloom in subarctic northeast Pacific, *Geophys. Res. Lett.*, 37, doi:10.1029/2010GL044629, 2010. [25](#)

- Humphreys, W. J.: Volcanic dust and other factors in the production of climatic changes, and their possible relation to ice ages, *Journal of the Franklin Institute*, 176, 131–172, 1913. [4](#)
- Jansen, E., Overpeck, J., Briffa, K., Duplessy, J.-C., Joos, F., Masson-Delmotte, V., Olago, D., Otto-Bliesner, B., Peltier, W., Rahmstorf, S., Ramesh, R., Raynaud, D., Rind, D., Solomina, O., Villalba, R., and Zhang, D.: Palaeoclimate, in: *Climate Change 2007: The Physical Science Basis. Contribution of Working Group I to the Fourth Assessment Report of the Intergovernmental Panel on Climate Change*, edited by Solomon, S., Qin, D., Manning, M., Chen, Z., Marquis, M., Averyt, K. B., Tignor, M., and Miller, H. L., pp. 434 – 497, Cambridge University Press, Cambridge, United Kingdom and New York, NY, USA, 2007. [28](#)
- Jones, C. D. and Cox, P. M.: Modelling the volcanic signal in the atmospheric CO<sub>2</sub> record, *Global Biogeochem. Cycles*, 15, 453–465, 2001. [4](#), [6](#), [26](#)
- Joos, F. and Prentice, I. C.: A paleo-perspective on changes in atmospheric CO<sub>2</sub> and climate, in: *The Global Carbon Cycle Integrating Humans, Climate and the Natural World*, edited by Field, C. B. and Raupach, M. R., pp. 165–186, SCOPE series, 2004. [11](#), [16](#), [28](#)
- Juus, F., Plattner, G.-K., Stocker, T. F., Marchal, O., and Schmittner, A.: Global warming and marine carbon cycle feedbacks on future atmospheric CO<sub>2</sub>, *Science*, 284, 464 – 467, doi:10.1126/science.284.5413.464, 1999. [26](#)
- Jungclauss, J. H., Lorenz, S. J., Timmreck, C., Reick, C. H., Brovkin, V., Six, K., Segschneider, J., Giorgetta, M. A., Crowley, T. J., Pongratz, J., Krivova, N. A., Vieira, L. E., Solanki, S. K., Klocke, D., Botzet, M., Esch, M., Gayler, V., Haak, H., Raddatz, T. J., Roeckner, E., Schnur, R., Widmann, H., Claussen, M., Stevens, B., and Marotzke, J.: Climate and carbon-cycle variability over the last millennium, *Clim. Past*, pp. 723–737, doi:10.5194/cp-6-723-2010, 2010. [28](#)
- Knorr, W.: Is the airborne fraction of anthropogenic carbon dioxide increasing?, *Geophys. Res. Lett.*, 36, doi:10.1029/2009GL040613, 2009. [3](#)
- Le Quéré, C., Raupach, M. R., Canadell, J. G., Marland, G., Bopp, L., Ciais, P., Conway, T. J., Doney, S. C., Feely, R., Foster, P., Friedlingstein, P., Gurney, K., Houghton, R. A., House, J. I., Huntingford, C., Levy, P. E., Lomas, M. R., Majkut, J., Metzl, N., Ometto, J. P., Peters, G. P., Prentice, I. C., Randerson, J. T., Running, S. W., Sarmiento, J. L., Schuster, U., Sitch, S., Viovy, T. T. N., van der Werf, G. R., and Woodward, F. I.: Trends in the sources and sinks of carbon dioxide, *Nature Geosciences*, 2, 831–836, doi:10.1038/ngeo689, 2009. [3](#)
- Lin, I.-I., Hu, C., Li, Y.-H., Ho, T.-Y., Fischer, T. P., Wong, G. T. F., Wu, J., Huang, C.-W., Chu, D. A., Ko, D. S., and Chen, J.-P.: Fertilization potential of volcanic dust in the low-nutrient low-chlorophyll western North Pacific subtropical gyre: Satellite evidence and laboratory study, *Global Biogeochem.*

Cycles, 25, GB1006, doi:10.1029/2009GB003758, 2011. 25

Lucht, W., Prentice, I. C., Myneni, R. B., Stith, S., Friedlingstein, P., Cramer, W., Bousquet, P., Buermann, W., and Smith, B.: Climatic control of the high-latitude vegetation greening trend and Pinatubo effect, *Science*, 296, 1687–1689, doi:10.1126/science.1071828, 2002. 5, 27

5 Meehl, G. A., Stocker, T. F., Collins, W. D., Friedlingstein, P., Gaye, A. T., Gregory, J. M., Kitoh, A., Knutti, R., Murphy, J. M., Noda, A., Raper, S. C. B., Watterson, I. G., Weaver, A. J., and Zhao, Z.-C.: Global Climate Projections, in: *Climate Change 2007: The Physical Science Basis. Contribution of Working Group I to the Fourth Assessment Report of the Intergovernmental Panel on Climate Change*, edited by Solomon, S., Qin, D., Manning, M., Chen, Z., Marquis, M., Averyt, K. B., Tignor, M., and Miller, H. L., pp. 747–845, Cambridge University Press, Cambridge, United Kingdom and New York, NY, USA, 2007. 3, 8, 23, 27

Mercado, L. M., Bellouin, N., Stith, S., Boucher, O., Huntingford, C., Wild, M., and Cox, P. M.: Impact of changes in diffuse radiation on the global land carbon sink, *Nature*, 458, 1014–1018, doi: 10.1038/nature07949, 2009. 25

15 Metzl, N., Corbière, A., Reverdin, G., Lenton, A., Takahashi, T., Olsen, A., Johannessen, T., Pierrot, D., Wanninkhof, R., Ólafsdóttir, S. R., Ólafsson, J., and Ramonet, M.: Recent acceleration of the sea surface fCO<sub>2</sub> growth rate in the North Atlantic subpolar gyre (1993–2008) revealed by winter observations, *Global Biogeochem. Cycles*, 24, GB4004, doi:10.1029/2009GB003658, 2010. 27

20 Najjar, R. G., Jin, X., Louanchi, F., Aumont, O., Caldeira, K., Doney, S. C., Dutay, J. C., Follows, M., Gruber, N., Joos, F., Lindsay, K., Maier-Reimer, E., Matear, R. J., Matsumoto, K., Monfray, P., Mouchet, A., Orr, J. C., Plattner, G. K., Sarmiento, J. L., Schlitzer, R., Slater, R. D., Weirig, M. F., Yamanaka, Y., and Yool, A.: Impact of circulation on export production, dissolved organic matter, and dissolved oxygen in the ocean: Results from Phase II of the Ocean Carbon-Cycle Model Intercomparison Project (OCMIP-2), *Global Biogeochem. Cycles*, 21, doi:10.1029/2006GB002857, 25 2007. 8

Orr, J. C., Fabry, V. J., Aumont, O., Bopp, L., Doney, S. C., Feely, R. M., Gnanadesikan, A., Gruber, N., Ishida, A., Joos, F., Key, R. M., Lindsay, K., Maier-Reimer, E., Matear, R. J., Monfray, P., Mouchet, A., Najjar, R. G., Plattner, G.-K., Rodgers, K. B., Sabine, C. L., Sarmiento, J. L., Schlitzer, R., Slater, R. D., Totterdell, I. J., Weirig, M.-F., Yamanaka, Y., and Yool, A.: Anthropogenic ocean acidification over the twenty-first century and its impact on marine calcifying organisms, *Nature*, 437, 681–686, doi:10.1038/nature04095, 2005. 29

30 Pérez, F. F., Vázquez-Rodríguez, M., Louarn, E., Padin, X. A., Mercier, H., and Rios, A. F.: Temporal variability of the anthropogenic CO<sub>2</sub> storage in the Irminger Sea, *Biogeosciences*, 5, 1669–1679,

doi:10.5194/bg-5-1669-2008, 2008. 27

- Plattner, G.-K., Knutti, R., Joos, F., Stocker, T. F., von Bloh, W., Brovkin, V., Cameron, D., Driesschaert, E., Dutkiewicz, S., Eby, M., Edwards, N. R., Fichefet, T., Hargreaves, J. C., Jones, C. D., Loutre, M. F., Matthews, H. D., Mouchet, A., Müller, S. A., Nawrath, S., Price, A., Sokolov, A., Strassmann, K. M., and Weaver, A. J.: Long-term climate commitments projected with climate - carbon cycle models, *J. Climate*, 21, 2721–2751, doi:10.1175/2007JCLI1905.1, 2008. 3, 10, 12, 16, 17, 28
- Randerson, J. T., Thompson, M. V., Conway, T. J., Fung, I. Y., and Field, C. B.: The contribution of terrestrial sources and sinks to trends in the seasonal cycle of atmospheric carbon dioxide, *Global Biogeochem. Cycles*, 11, 535–560, 1997. 7
- Robock, A.: Volcanic eruptions and climate, *Rev. Geophys.*, 38, 191–219, 2000. 4, 5
- Robock, A. and Mao, J.: Winter warming from large volcanic eruptions, *Geophys. Res. Lett.*, 12, 2405–2408, 1992. 19
- Robock, A., Oman, L., and Stenchikov, G.: Regional climate responses to geoengineering with tropical and Arctic SO<sub>2</sub> injections, *J. Geophys. Res.*, 113, D16 101, doi:10.1029/2008JD010050, 2008. 19, 29
- Rödenbeck, C., Houweling, S., Gloor, M., and Heimann, M.: CO<sub>2</sub> flux history 1982-2001 inferred from atmospheric data using a global inversion of atmospheric transport, *Atmos. Chem. Phys.*, 3, 1919–1964, doi:10.5194/acp-3-1919-2003, 2003. 5
- Roy, T., Bopp, L., Gehlen, M., Schneider, B., Cadule, P., Frölicher, T. L., Segschneider, J., Tjiputra, J., Heinze, C., and Joos, F.: Regional impacts of climate change and atmospheric CO<sub>2</sub> on future ocean carbon uptake: A multi-model linear feedback analysis, *J. Clim.*, (in press), 2011. 12
- Royal Society: Geoengineering the climate, Policy Report 09/09, Royal Society, London, 2009. 29
- Sarmiento, J. L., Gloor, M., Gruber, N., Beaulieu, C., Jacobson, A. R., Fletcher, S. E. M., Pacala, S. W., and Rodgers, K. B.: Trends and regional distributions of land and ocean carbon sinks, *Biogeosciences*, 7, doi:10.5194/bg-7-2351-2010, 2010. 3, 5, 26
- Scheffer, M., Brovkin, V., and Cox, P. M.: Positive feedback between global warming and atmospheric CO<sub>2</sub> concentration inferred from past climate change, *Geophys. Res. Lett.*, 33, L10 702, doi:10.1029/2005GL025044, 2006. 11, 12, 16, 28
- Schmidt, G. A., Jungclaus, J. H., Ammann, C. M., Bard, E., Braconnot, P., Crowley, T. J., Delaygue, G., Joos, F., Krivova, N. A., Muscheler, R., Otto-Bliesner, B. L., Pongratz, J., Shindell, D. T., Solanki, S. K., Steinhilber, F., and Vieira, L. E. A.: Climate forcing reconstructions for use in PMIP simulations of the last millennium (v1.0), *Geosci. Model. Dev.*, 4, 33–45, doi:10.5194/gmd-4-33-2011, 2011. 29
- Schuster, U. and Watson, A. J.: A variable and decreasing sink for atmospheric CO<sub>2</sub> in the North Atlantic, *J. Geophys. Res.*, 112, C11 006, doi:10.1029/2006JC003941, 2007. 27

- Schuster, U., Watson, A. J., Bates, N. R., Corbière, A., Gonzalez-Davila, M., Metzl, N., Pierrot, D., and Santana-Casiano, M.: Trends in North Atlantic sea-surface fCO<sub>2</sub> from 1990 to 2006, *Deep-Sea Res. II*, 56, 620–629, doi:10.1016/j.dsr2.2008.12.011, 2009. 27
- Shindell, D. T., Schmidt, G. A., Mann, M. E., and Faluvegi, G.: Dynamic winter climate response to large tropical volcanic eruptions since 1600, *J. Geophys. Res.*, 109, D05 104, doi:10.1029/2003JD004151, 2004. 5, 8, 18
- Siegenthaler, U.: Biogeochemical cycles - El-Niño and atmospheric CO<sub>2</sub>, *Nature*, 345, 295–296, 1990. 3
- Steinacher, M., Joos, F., Frölicher, T. L., Plattner, G.-K., and Doney, S. C.: Iminent ocean acidification in the Arctic projected with the NCAR global coupled carbon cycle-climate model, *Biogeosciences*, 6, 515–533, 2009. 8
- Steinacher, M., Joos, F., Frölicher, T. L., Bopp, L., Cocco, V., Cadule, P., Doney, S. C., Gehlen, M., Lindsay, K., Moore, J., Schneider, B., and Segschneider, J.: Projected 21st century decrease in marine productivity: a multi-model analysis, *Biogeosciences*, 7, 979–1005, 2010. 8, 22
- Stenchikov, G., Hamilton, K., Stouffer, R. J., Robock, A., Ramaswamy, V., Santer, B., and Graf, H.-F.: Arctic Oscillation response to volcanic eruptions in the IPCC AR4 climate models, *J. Geophys. Res.*, 111, doi:10.1029/2005JD006286, 2006. 8
- Stenchikov, G., Delworth, T. L., Ramaswamy, V., Stouffer, R. J., Wittenberg, A., and Zeng, F.: Volcanic signals in oceans, *J. Geophys. Res.*, 114, doi:10.1029/2008JD011673, 2009. 5, 15, 27
- Thomas, H., Prowe, A. E. F., Lima, I. D., Doney, S. C., Wanninkhof, R., Greatbatch, R. J., Schuster, U., and Corbière, A.: Changes in the North Atlantic Oscillation influence CO<sub>2</sub> uptake in the North Atlantic over the past 2 decades, *Global Biogeochem. Cycles*, 22, doi:10.1029/2007GB003167, 2008. 27
- Thompson, D. W. J., Wallace, J. M., Jones, P. D., and Kennedy, J. J.: Identifying signatures of natural climate variability in time series of global-mean surface temperature: Methodology and insights, *J. Climate*, 22, doi:10.1175/2009JCLI3089.1, 2009. 4
- Timmreck, C., Graf, H.-F., Lorenz, S. J., Niemeier, U., Zanchettin, D., Matei, D., Jungclaus, J. H., and Crowley, T. J.: Aerosol size confines climate response to volcanic super-eruptions, *Geophys. Res. Lett.*, 37, doi:10.1029/2010GL045464, 2010. 25
- Watson, A.: Volcanic iron, CO<sub>2</sub>, ocean productivity and climate, *Nature*, 385, 587–588, doi:10.1038/385587b0, 1997. 25
- Wigley, T. M. L.: The climate change commitment, *Science*, 307, 1766–1769, doi:10.1126/science.1103934, 2005. 14

- Wigley, T. M. L.: A combined mitigation/geoengineering approach, *Science*, 314, 452–454, doi:10.1126/science.1131728, 2006. 29
- Yoshimori, M., Stocker, T. F., Raible, C. C., and Renold, M.: Externally forced and internal variability in ensemble climate simulations of the Maunder Minimum, *J. Climate*, 18, 4253–4270, 2005. 4

**Table 1.** Overview of all experiments, the magnitude of Pinatubo scaling, and the lengths of the simulations. All experiments are started from nearly steady state preindustrial conditions using the same initial conditions.

Experiment	Pinatubo scaling	Period / Years
Control	-	280
Scaling experiments		
Pin.1x	1	20
Pin.2x	2	20
Pin.5x	5	20
Pin.10x	10	20
Pin.20x	20	20
Pin.50x	50	20
Pin.100x	100	20
Transient experiments		
Volc	Historical volcanoes	1820-2099
No.volc	-	1820-2099

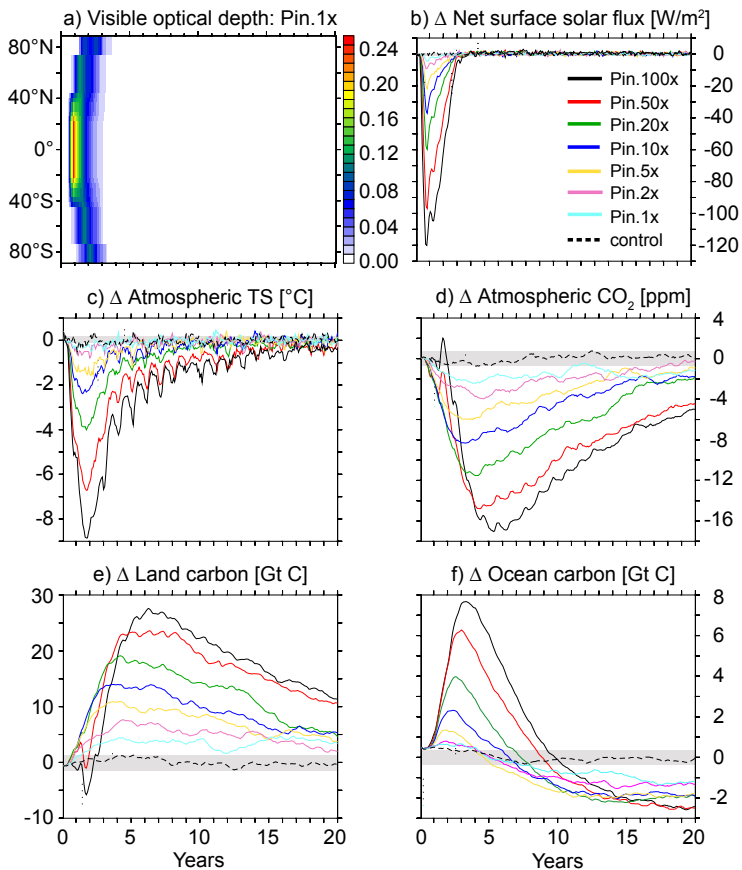


**Fig. 1.** (a) Prescribed zonal averaged stratospheric optical depth in the mid-visible wavelength for the Pin.1x case. (b-f) Global mean responses of the carbon cycle-climate system to different strengths of volcanic eruptions: time series of monthly (b) net surface solar flux, (c) atmospheric surface temperature, (d) atmospheric  $\text{CO}_2$  concentration, (e) land carbon inventory and (f) ocean carbon inventory (sum of dissolved inorganic and organic carbon). In all plots in (b-f) and for all cases, the mean annual cycle from the control simulation has been removed. The volcanic eruptions start after half a year. The grey bar shows one standard deviation from a 280-yr control simulation. The control simulation has first been detrended with a 50-yr spline before calculating one standard deviation for the land and ocean carbon inventory to remove the artificial long-term drift.

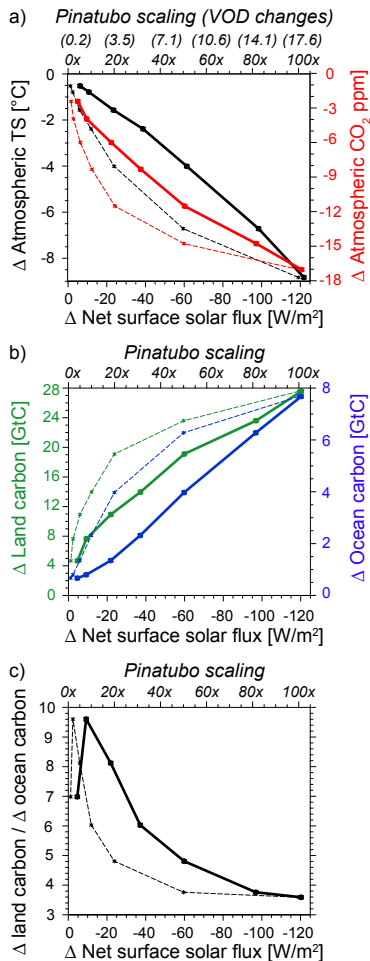


**Fig. 2.** (a) Peak changes in surface atmospheric temperature (black) and surface atmospheric CO<sub>2</sub> (red) as a function of the Pinatubo scaling (dashed line) and the peak changes in net surface solar flux (solid line), respectively. Aerosol optical depth changes in the mid-visible wavelength (VOD) for the different Pinatubo scalings are also given in brackets (top abscissa). (b,c) The same as in (a) but for (b) land carbon changes (green lines) and ocean carbon changes (blue lines) as well as for (c) the ratio between peak changes in land carbon and ocean carbon.

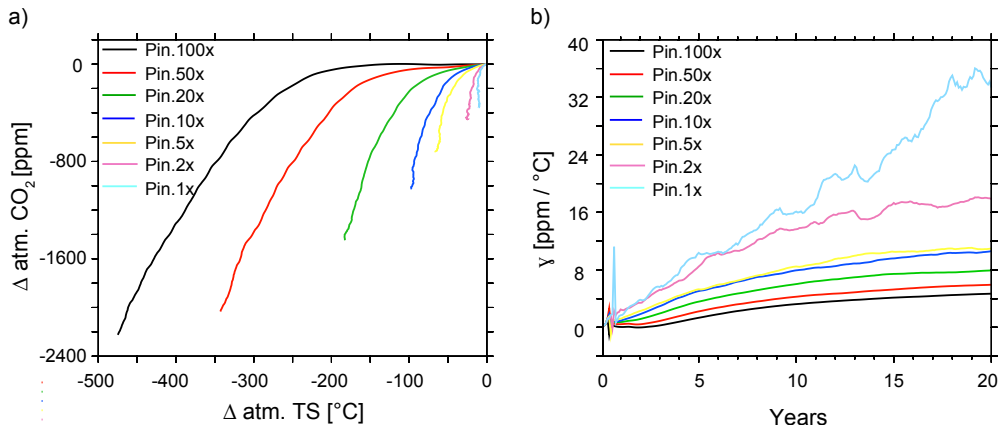


**Fig. 3.** (a) Simulated cumulative temporal mean changes in atmospheric CO<sub>2</sub> vs. temporal mean changes in atmospheric surface temperature for different Pinatubo scalings. The point values leading to the curves are time integrals of the data in Fig. 1c and Fig. 1d. Note that the ratio of the cumulative values equals the ratio of time averaged values and thus climate-carbon sensitivity  $\gamma$  defined by equation 5 and shown in panel b; the larger the slope of the curve the larger  $\gamma$ . (b) Time-series of estimates of the climate-carbon cycle sensitivity  $\gamma$  derived from the Pinatubo scaling experiments.

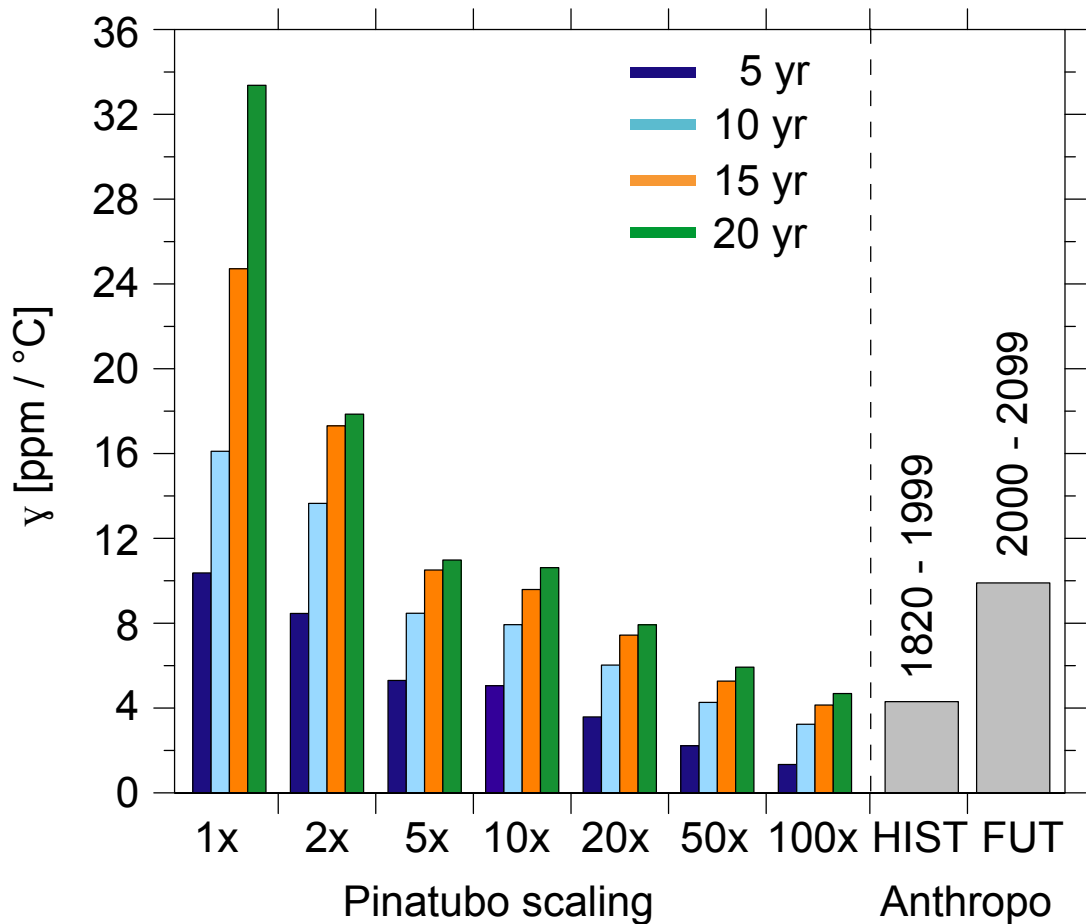


**Fig. 4.** Estimates of climate-carbon cycle sensitivity  $\gamma$  derived from the Pinatubo scaling experiments (labeled as Pinatubo scaling) and from transient simulations over the period 1820 to 2099 (labeled as Anthropo) with the NCAR CSM1.4-carbon model. Colors indicate the considered time scales, indicated by the labels 5yr, 10yr, 15yr and 20yr. Grey bars show  $\gamma$ 's calculated from transient simulations forced with historical carbon emissions over the period 1820 to 1999 (HIST: 1820-1999) and following the SRES A2 scenario over the period 2000 to 2099 (FUT: 2000-2099), respectively.

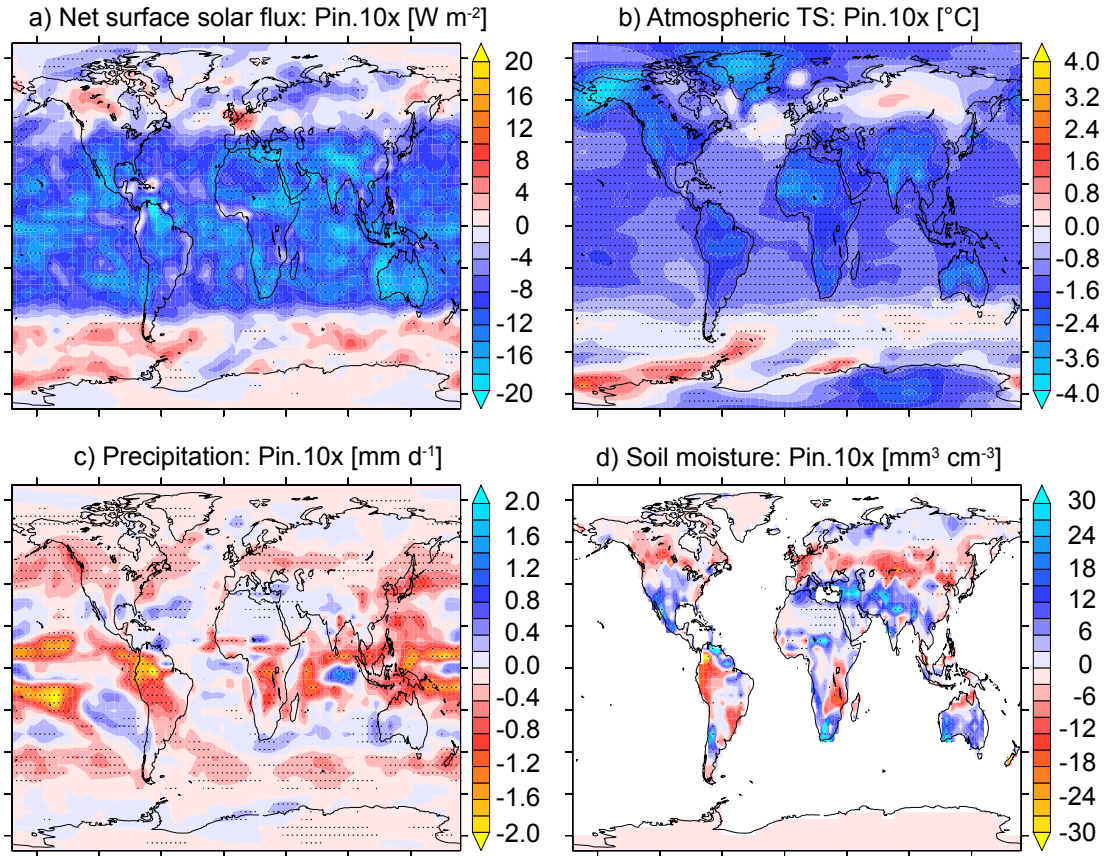


**Fig. 5.** Difference pattern between the Pin.10x case and the control simulation averaged over the first 5 years: (a) net surface solar flux changes, (b) atmospheric surface temperature changes, (c) precipitation changes, and (d) soil moisture changes. Stippling in (a-d) denotes grid cells where the changes are significant at the 5% level based on the two sided Student's t-test.

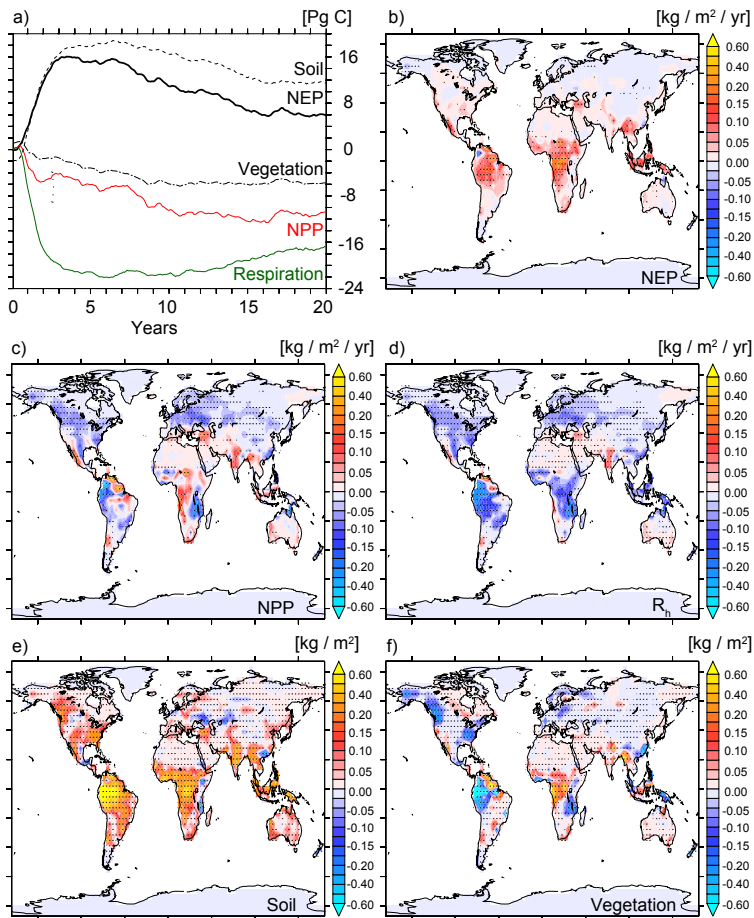
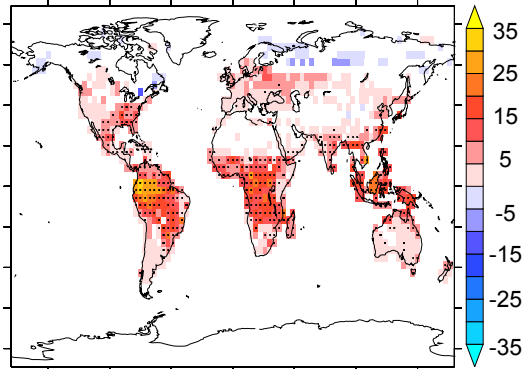
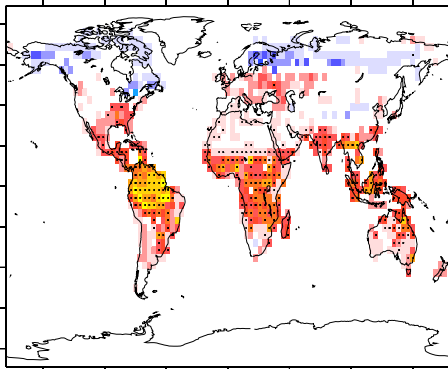


**Fig. 6.** Evolution of land carbon inventory changes and associated mechanism. (a) Monthly, deseasonalized anomalies of soil and vegetation carbon inventories (black dashed lines), time-integrated NEP (solid black), NPP (red) and  $R_h$  (green) for the Pin.10x case. (b-f) Changes in (b) NEP, (c) NPP, (d)  $R_h$ , (e) soil carbon inventory, and (f) vegetation carbon inventory averaged over the first 5 years for the Pin.10x case. Net ecosystem production (NEP) is the difference between NPP and  $R_h$ . Stippling in (b-f) denotes grid cells where the magnitude of changes are significant at the 5% level based on a two-sided Student's t-test.

a) NPP [g/m<sup>2</sup>/day] vs. soil moisture [mm<sup>3</sup>/mm<sup>3</sup>]

b) R<sub>h</sub> [g/m<sup>2</sup>/day] vs. soil moisture [mm<sup>3</sup>/mm<sup>3</sup>]



c) NPP [g/m<sup>2</sup>/day] vs. temperature [°C]

d) R<sub>h</sub> [g/m<sup>2</sup>/day] vs. temperature [°C]

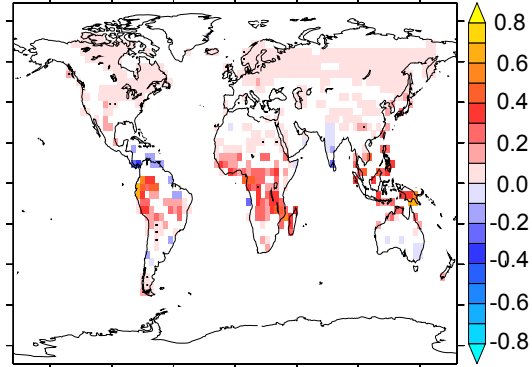
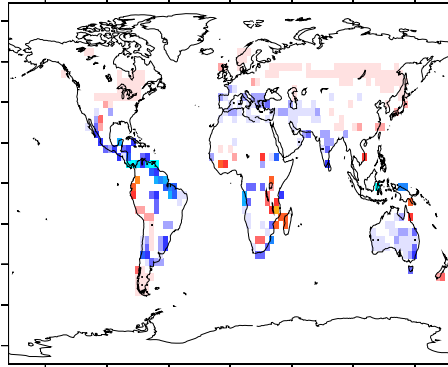


**Fig. 7.** Linear regression analysis of deseasonalized NPP (a,c) and R<sub>h</sub> (b,d) on (a,b) deseasonalized soil moisture and (c,d) surface temperature for the Pin.10x case. Color shading represents the sensitivity of NPP and R<sub>h</sub> to these variables (slopes of the linear regression). The regression has been calculated over the first 5 years and only grid cells where  $r^2 > 0.1$  are shown. Stippling denotes correlations with  $r^2 > 0.5$ .

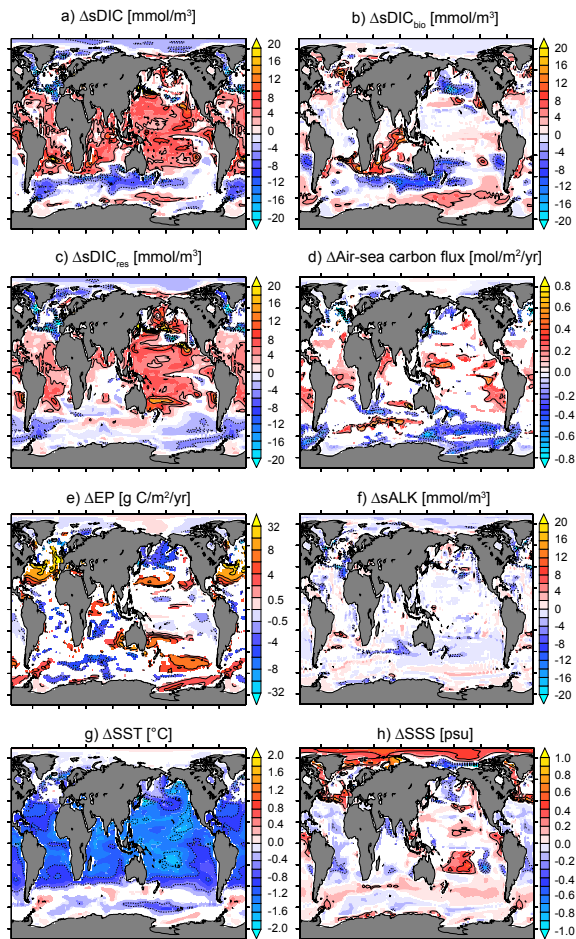


**Fig. 8.** Difference pattern between the Pin.10x case and the control simulation averaged over the first 5 years: (a) sea surface sDIC, (b) sea surface sDIC changes due to the internal reorganization of the organic matter cycle and CaCO<sub>3</sub> cycle ( $sDIC_{bio}$ ), (c) the residual sDIC ( $sDIC_{res} = sDIC - \Delta sDIC_{bio}$ ), (d) air-sea carbon flux, (e) export production of particulate organic carbon, (f) sALK, (g) sea surface temperature and (h) sea surface salinity. Only grid cells are shown where the magnitude of changes are significant at the 5% level based on a two-sided Student's t-test. The changes for export production are shown on an exponential scale.

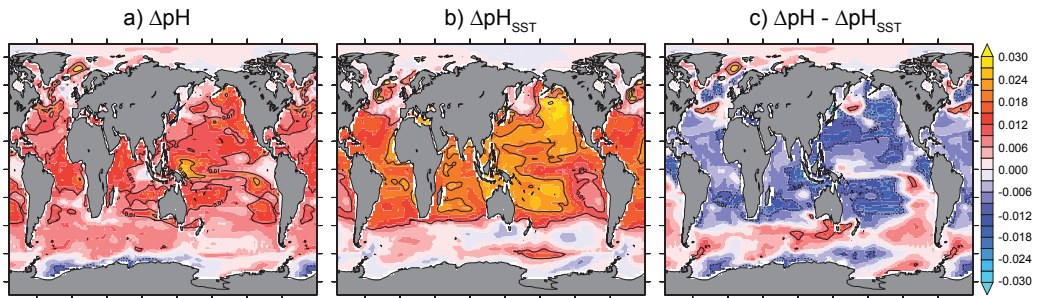


**Fig. 9.** Difference pattern between the Pin.10x case and the control simulation averaged over the first 5 years: (a) pH changes, (b) pH due to changes in SST only and (c) pH changes not caused by SST changes.

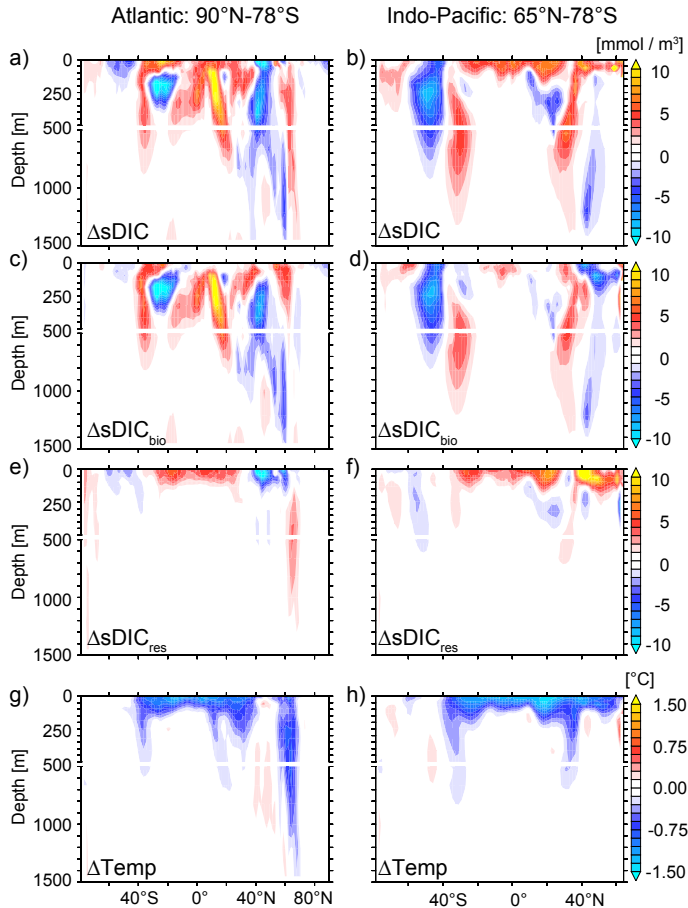


**Fig. 10.** Zonal mean differences between the Pin.10x case and the control simulation in the Atlantic Ocean (including the Arctic Ocean; a,c,e,g) and the Indo-Pacific Ocean (b,d,f,h): (a-b) sDIC, (c-d) sDIC changes due to the internal reorganization of the organic matter cycle and  $CaCO_3$  cycle ( $sDIC_{bio}$ ), (e-f) the residual sDIC ( $sDIC_{res}=sDIC-\Delta sDIC_{bio}$ ), and (g-h) potential temperature. All panels show results averaged over the first 5 years of the simulations. Changes in zonal mean sDIC are significant almost everywhere in the top 1500 m (not shown).

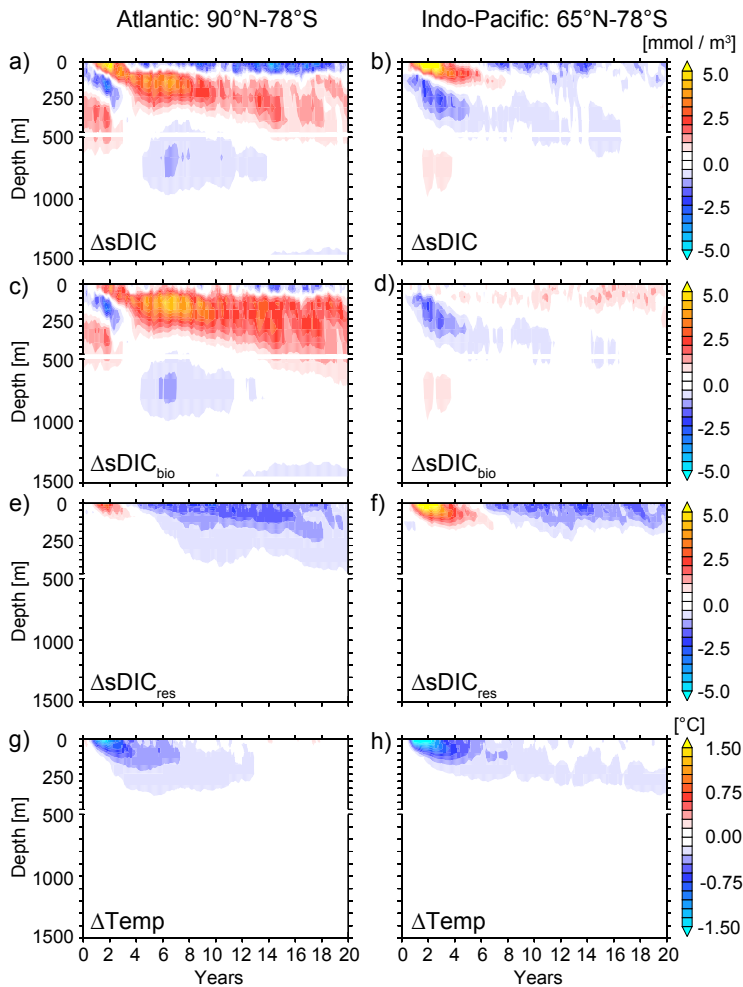


**Fig. 11.** Hovmöller diagram of monthly mean  $sDIC$ ,  $sDIC_{bio}$ ,  $sDIC_{res}$  and potential temperature differences between the Pin.10x case and the control simulation in the Atlantic (including the Arctic Ocean; a,c,e,g) and the Indo-Pacific Ocean (b,d,f,h) at different depths. The volcanic eruption starts in year 0.5.

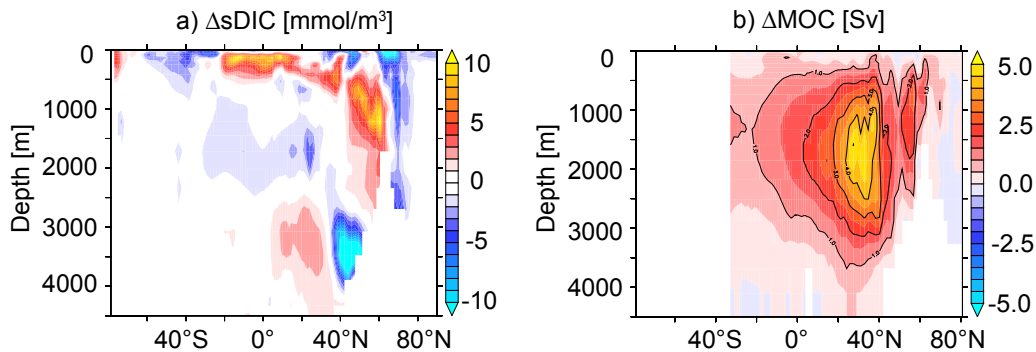


**Fig. 12.** Meridional section through the Atlantic Ocean including the Arctic Ocean showing the simulated zonal mean differences in (a) sDIC and (b) the meridional overturning circulation between the Pin.10x case and the control simulation averaged over the last 5 years (years 16-20). Contours in (b) are every 1 Sv.

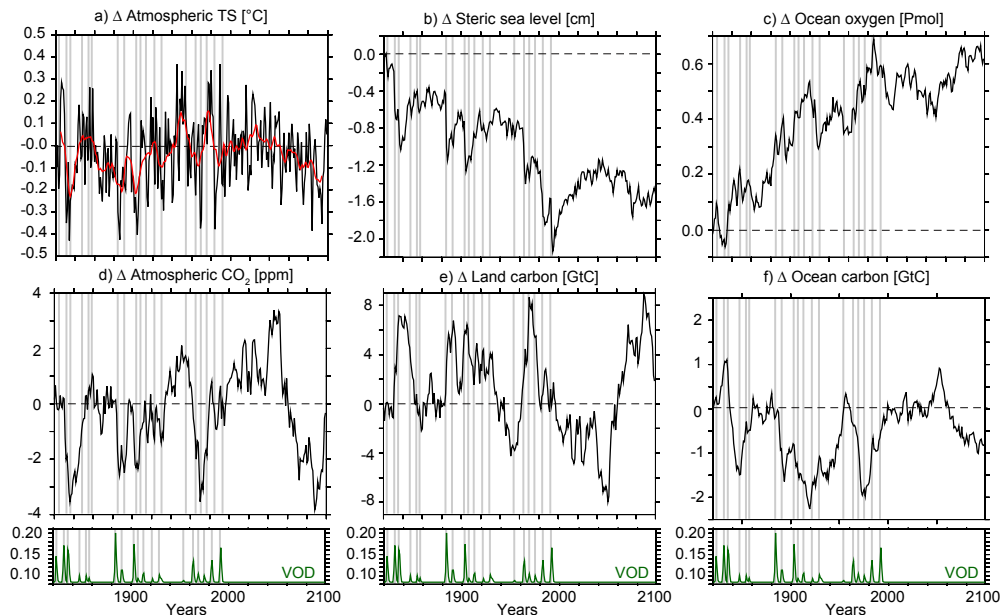


**Fig. 13.** Differences in global annual mean (a) atmospheric surface temperature, (b) steric sea level, (c) ocean oxygen inventory, (d) atmospheric CO<sub>2</sub>, (e) land carbon inventory, and (f) ocean carbon inventory between a simulation with and a simulation without volcanic eruptions over the period 1820 to 2099. (Bottom) Volcanic forcing expressed as aerosol optical depth changes in the mid-visible wavelength (VOD). The gray shaded bands indicate different historical explosive volcanic eruptions. No volcanic eruptions are assumed for the period 2000 to 2099. Dashed lines show the zero-line as reference. Red line in (a) shows the 10-yr running mean of atmospheric surface temperature differences to highlight decadal changes.

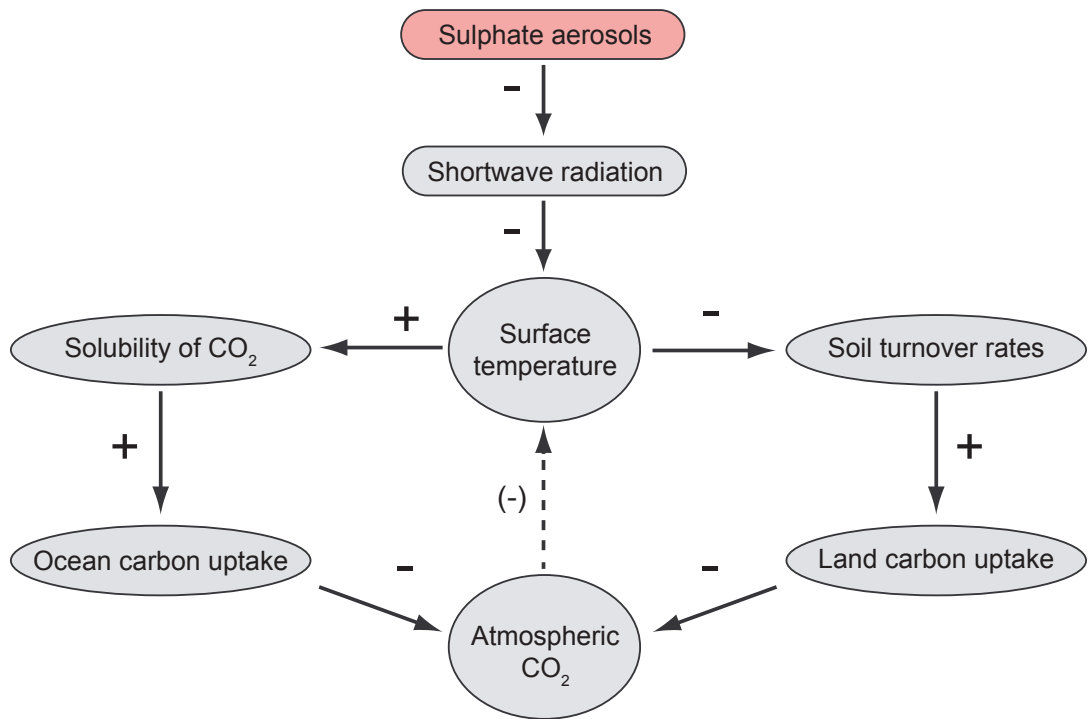


**Fig. 14.** Flowchart of changes after an explosive volcanic eruption. The small impact of enhanced mixing and export production, and decreased stratification on air-sea gas exchange as well as the impact of precipitation and diffuse radiation on NPP are neglected here. The dashed arrow shows the small amplifying feedback for climate change.